Chapter 3

Semiclassical Mechanics of Diatomic Rotors in Tilted Fields

3.1 Semiclassical Rotational Excitation of Diatomic Rotors in Linearly Polarized Intense Laser Pulses

The rotational excitation studied here is caused by an intense, high frequency and linearly polarized laser pulse. The frequency of the radiation is high compared with the rotational frequency of the system and so the interaction between the laser and the rotor is treated as a time average over a cycle of the laser field [10].

3.1.1 Classical Description of the System

In terms of the action-angle variables for the free rotor the Hamiltonian of the system is

$$H = Bj^2 - g(t)\Delta\omega\left(1 - \frac{m^2}{j^2}\right)\cos^2 q_j, \tag{3.1}$$

where $B = 1/2I$ is the rotational constant, j and m are the magnitude and the z-component (respectively) of the angular momentum vector $\boldsymbol{j}$, and $g(t)$ is the envelope function for the intensity of the laser pulse. In the present case the envelope function is a Gaussian pulse

$$g(t) = \exp\left[-\frac{(t-t_0)^2}{\sigma^2}\right]. \tag{3.2}$$

This laser pulse has maximum intensity at t_0 and full-width at half-maximum $\tau \approx (5/3)\sigma$ [73].

Since q_m is absent in this Hamiltonian, m is a constant of the motion. For $m = j$ the molecule is rotating in a plane perpendicular to the laser polarization. The $m = 0$ case is particularly simply to study; here the molecule will librate or rotate in a vertical plane passing through the poles. For $m = 0$ the Hamiltonian simplifies to

$$H = Bj^2 - g(t)\Delta\omega \cos^2 \varphi, \tag{3.3}$$

where φ is used instead of q_j. Although $\varphi = q_j$ depends of the sense of rotation, in this 2D-model it is a simple polar angle. This time-dependent system can be studied in the extended phase space (j, φ, t, p_t) with effective Hamiltonian

$$K = Bj^2 - g(t)\Delta\omega \cos^2 \varphi + p_t. \tag{3.4}$$

Now the role of the t is played by the auxiliary progress parameter s, so that the canonical equations are:

$$\frac{\mathrm{d}t}{\mathrm{d}s} = \frac{\partial K}{\partial p_t} = 1, \tag{3.5a}$$

$$\frac{\mathrm{d}p_t}{\mathrm{d}s} = -\frac{\partial K}{\partial t} = -\frac{2\Delta\omega(t - t_0)}{\sigma^2} g(t) \cos^2 \varphi, \tag{3.5b}$$

$$\frac{\mathrm{d}\varphi}{\mathrm{d}s} = \frac{\partial K}{\partial j} = 2Bj, \tag{3.5c}$$

$$\frac{\mathrm{d}j}{\mathrm{d}s} = -\frac{\partial K}{\partial \varphi} = -g(t)\Delta\omega \sin 2\varphi. \tag{3.5d}$$

Since the Hamiltonian K is explicitly independent of s its value must be a constant of motion. For $K = 0$ equation (3.4) gives

$$p_t = -Bj^2 + g(t)\Delta\omega \cos^2 \varphi, \tag{3.6}$$

which gives the energy of the system at any time and provides the initial condition for p_t.

3.1.2 Classical Interaction Picture

The form of the Hamiltonian (3.3) allows the separation

$$H = H_0(j) + H_1(\varphi, t), \tag{3.7}$$

where H_0 is the free 2D-rotor Hamiltonian and H_1 contains the interaction with the pulse. In the classical interaction picture (CIP) the dynamical variables evolve forward in time according to the full Hamiltonian H then backward in time using the Hamiltonian H_0 [74].

The Hamiltonian in the CIP is obtained by a canonical transformation using an $F_3(j, \bar{\varphi}; t)$ generator, which is an explicit function of the old momentum j, the new angle $\bar{\varphi}$, and the time t,

$$F_3(j, \bar{\varphi}; t) = -j\bar{\varphi} - Bj^2 (t - t_0) . \tag{3.8}$$

For this generating function [20]

$$\bar{j} = -\frac{\partial F_3}{\partial \bar{\varphi}} = j, \tag{3.9a}$$

$$\varphi = -\frac{\partial F_3}{\partial j} = \bar{\varphi} + 2Bj (t - t_0) , \tag{3.9b}$$

$$\bar{H} = H + \frac{\partial F_3}{\partial t} H - Bj^2 = -g(t)\Delta\omega \cos^2 [\bar{\varphi} + 2Bj (t - t_0)]. \tag{3.9c}$$

which give the new momentum $\bar{j}$, the old angle φ, and the new Hamiltonian $\bar{H}$.

For the Hamiltonian (3.9c) the equations of motion are

$$\frac{\mathrm{d}\bar{\varphi}}{\mathrm{d}t} = \frac{\partial \bar{H}}{\partial j} = 2B (t - t_0) g(t)\Delta\omega \sin 2 [\bar{\varphi} + 2Bj (t - t_0)], \tag{3.10a}$$

$$\frac{\mathrm{d}j}{\mathrm{d}t} = -\frac{\partial \bar{H}}{\partial \bar{\varphi}} = -g(t)\Delta\omega \sin 2 [\bar{\varphi} + 2Bj (t - t_0)], \tag{3.10b}$$

and for the extended phase space the additional equation

$$\begin{aligned} \frac{\mathrm{d}p_t}{\mathrm{d}t} = -\frac{\partial \bar{H}}{\partial t} =& g'(t)\Delta\omega \cos^2 [\bar{\varphi} + 2Bj (t - t_0)] \\ & - 2Bjg(t)\Delta\omega \sin 2 [\bar{\varphi} + 2Bj (t - t_0)]. \end{aligned} \tag{3.11}$$

3.1.3 Stability Matrix

The equation of motion for the stability matrix M is (see appendix C)

$$\frac{\mathrm{d}\mathsf{M}}{\mathrm{d}t} = \mathsf{JHM}, \tag{3.12}$$

with J the symplectic matrix, and H the Hessian matrix of the Hamiltonian.

For the Hamiltonian (3.9c) the components of the Hessian matrix H are

$$\frac{\partial^2 \bar{H}}{\partial \varphi^2} = 2g(t)\Delta\omega \cos 2\left[\bar{\varphi} + 2Bj\,(t - t_0)\right], \tag{3.13a}$$

$$\frac{\partial^2 \bar{H}}{\partial j \partial \varphi} = 2B\,(t - t_0)\, g(t)\Delta\omega \cos 2\left[\bar{\varphi} + 2Bj\,(t - t_0)\right], \tag{3.13b}$$

$$\frac{\partial^2 \bar{H}}{\partial j^2} = \left[2B\,(t - t_0)\right]^2 g(t)\Delta\omega \cos 2\left[\bar{\varphi} + 2Bj\,(t - t_0)\right], \tag{3.13c}$$

$$\frac{\partial^2 \bar{H}}{\partial \varphi \partial j} = \frac{\partial^2 \bar{H}}{\partial j \partial \varphi}. \tag{3.13d}$$

3.1.4 Bohr-Sommerfeld Quantization Rules

Classically j and H can take any real value. For the quantum analog of this model j can take only integer values and the energy is proportional to the square of these integers. A simple semiclassical approach is to use the Bohr-Sommerfeld (BS) quantization rule [75] for the values of J

$$j = M\hbar, \qquad M \in \mathbb{Z}, \tag{3.14}$$

the energy levels are given by

$$\begin{aligned} E &= Bj^2 \\ &= BM^2\hbar^2, \qquad M \in \mathbb{Z}. \end{aligned} \tag{3.15}$$

From Heisenberg's uncertainty principle, precise knowledge of j implies complete ignorance of the angle variable φ. In classical terms the BS quantization

condition for the 2D-rotor is a line of constant j, given by equation (3.14), and all possible values of the angle φ.

For a sufficiently narrow Gaussian pulse, the system described by equation (3.3) is a free 2D-rotor for times $|t - t_0| \gg 0$. Rotational excitation can be studied observing the classical evolution of an ensemble of initial conditions given by the BS rule. After the pulse j becomes constant for all initial conditions. The initial conditions with quantized values of final j given by BS rules are considered in this semiclassical approach to rotational excitation. The trajectories associated with these initial conditions are called root trajectories. More explicitly, for a given root trajectory the rotor begins at $\boldsymbol{z}_i = (\varphi_i, j_i)$ with $j_i = M_i\hbar$, and ends up at $\boldsymbol{z}_f = (\varphi_f, j_f)$ with $j_f = M_f\hbar$, evolving along a trajectory $\boldsymbol{z}(\boldsymbol{z}_i; t) = (\varphi(\boldsymbol{z}_i; t), j(\boldsymbol{z}_i; t))$. Sometimes the notation $\boldsymbol{z}_t(\boldsymbol{z}_i) = (\varphi_t(\boldsymbol{z}_i), j_t(\boldsymbol{z}_i))$ could be used for the trajectory.

3.1.5 Sudden Approximation

For short pulses the use of the sudden approximation is appropriate [76]. In this approximation the pre-to-post-pulse propagator for the Hamiltonian (3.3) can be written as [39]

$$\hat{U}(t) = \mathrm{e}^{\mathrm{i}\beta\cos^2\varphi}\mathrm{e}^{-\mathrm{i}t\hat{H}_0/\hbar}, \tag{3.16}$$

where $\hat{H}_0$ is the Hamiltonian for the free 2D-rotor and β is

$$\hbar\beta = -\int_0^t g(t')\Delta\omega \mathrm{d}t' = -\sqrt{\pi}\sigma\Delta\omega, \tag{3.17}$$

for the Gaussian pulse described by equation (3.2), with $0 < t_0 < t$ such that the pulse intensity is practically zero at the initial and final times. For the initial wave

function $\psi_0(\varphi) = (2\pi)^{-1/2}\mathrm{e}^{\mathrm{i}M_0\varphi}$, the wave function at time t is given by

$$\begin{aligned}\psi_t(\varphi) &= \hat{U}(t)\psi_0(\varphi) \\ &= \mathrm{e}^{\mathrm{i}\beta\cos^2\varphi}\mathrm{e}^{-\mathrm{i}tE_{M_0}/\hbar}\psi_0(\varphi)\end{aligned} \tag{3.18}$$

This wavefunction can be also expanded in terms of the 2D-rotor eigenfunctions $\psi_M(\varphi) = (2\pi)^{-1/2}\mathrm{e}^{\mathrm{i}M\varphi}$,

$$\psi_t(\varphi) = \sum_{M\in\mathbb{Z}} c_M(t)\psi_M(\varphi)\mathrm{e}^{-\mathrm{i}tE_M/\hbar}. \tag{3.19}$$

From equations (3.18) and (3.19) the coefficients of this expansion are

$$c_M(t) = \frac{1}{2\pi}\mathrm{e}^{\mathrm{i}t(E_M-E_{M_0})/\hbar}\int_0^{2\pi}\mathrm{e}^{\mathrm{i}\beta\cos^2\varphi}\mathrm{e}^{-\mathrm{i}\varphi\Delta M}\mathrm{d}\varphi, \tag{3.20}$$

with $\Delta M = M - M_0$. Using the trigonometric identity $2\cos^2\varphi = 1 + \cos 2\varphi$, and the change of variable $\varphi' = 2\varphi$, the integral can be recast as

$$\int_0^{2\pi}\mathrm{e}^{\mathrm{i}\beta\cos^2\varphi}\mathrm{e}^{-\mathrm{i}\varphi\Delta M}\mathrm{d}\varphi = \frac{\mathrm{e}^{\mathrm{i}\beta/2}}{2}\int_0^{4\pi}\mathrm{e}^{\mathrm{i}(\beta/2)\cos\varphi'}\mathrm{e}^{-\mathrm{i}\varphi'\Delta M/2}\mathrm{d}\varphi'. \tag{3.21}$$

The last integral can be expressed in terms of Bessel functions of the first kind,

$$J_n(z) = \frac{1}{2\pi\mathrm{i}^n}\int_0^{2\pi}\mathrm{e}^{\mathrm{i}z\cos\theta}\mathrm{e}^{\mathrm{i}n\theta}\mathrm{d}\theta, \qquad n\in\mathbb{Z}, \tag{3.22}$$

giving

$$\int_0^{4\pi}\mathrm{e}^{\mathrm{i}(\beta/2)\cos\varphi'}\mathrm{e}^{-\mathrm{i}\varphi'\Delta M/2}\mathrm{d}\varphi' = \frac{2\pi}{\mathrm{i}^{\Delta M/2}}J_{-\frac{\Delta M}{2}}(\beta/2) + \int_{2\pi}^{4\pi}\mathrm{e}^{\mathrm{i}(\beta/2)\cos\varphi'}\mathrm{e}^{-\mathrm{i}\varphi'\Delta M/2}\mathrm{d}\varphi'. \tag{3.23}$$

For the last integral the change of variable $\varphi'' = \varphi' - 2\pi$ gives

$$\int_{2\pi}^{4\pi}\mathrm{e}^{\mathrm{i}(\beta/2)\cos\varphi'}\mathrm{e}^{-\mathrm{i}\varphi'\Delta M/2}\mathrm{d}\varphi' = \frac{2\pi}{\mathrm{i}^{\Delta M/2}}\mathrm{e}^{-\mathrm{i}\pi\Delta M}J_{-\frac{\Delta M}{2}}(\beta/2). \tag{3.24}$$

Finally, the coefficient c_M is

$$c_M(t) = \mathrm{e}^{\mathrm{i}t(E_M-E_{M_0})/\hbar}\mathrm{e}^{\mathrm{i}\beta/2}\frac{1}{2\mathrm{i}^{\Delta M/2}}J_{-\frac{\Delta M}{2}}(\beta/2)\left(1+\mathrm{e}^{-\mathrm{i}\pi\Delta M}\right), \tag{3.25}$$

and the transition probability

$$\begin{aligned} P_{M_0\to M} &= |c_M(t)|^2 \\ &= \frac{1+\cos(\pi\Delta M)}{2}\left[J_{-\frac{\Delta M}{2}}(\beta/2)\right]^2. \end{aligned} \tag{3.26}$$

Thus within the sudden approximation if ΔM is odd then $P_{M_0\to M}=0$. For even ΔM, this equation can be written as

$$P_{M_0\to M} = \left[J_{\frac{\Delta M}{2}}(\beta/2)\right]^2, \qquad \Delta M \text{ even}, \tag{3.27}$$

resorting to $J_{-n}(z)=(-1)^n J_n(z)$.

The effectiveness of the sudden approximation for short pulses is shown in figure 3.1. For a pulse of width $\sigma=0.02$ and $M_0=0$, the figure shows an almost perfect agreement for all the transition probabilities for small $\Delta\omega$. For larger values of $\Delta\omega$ the results of the approximation are slightly different from the quantum transition probabilities [72]. For a longer pulse of width $\sigma=0.04$ the approximation works fine for $\Delta\omega<200$ and gets poor results as the value of $\Delta\omega$ increases.

3.1.6 Semiclassical Amplitude Formulas

The formulas derived in this section are valid for both the action-angle variables and the classical interaction picture. However, it is convenient to use the CIP for this specific time-dependent problem. For notational convenience the CIP angle is denoted by φ, rather than $\bar{\varphi}$.

The semiclassical amplitude in momentum representation is obtained from the initial momentum to final coordinate representation,

$$\langle j_f|\, \mathrm{e}^{-\mathrm{i}\hat{H}t/\hbar}\,|j_i\rangle = \int \mathrm{d}\varphi_f\, \langle j_f|\,\varphi_f\rangle\,\langle\varphi_f|\,\mathrm{e}^{-\mathrm{i}\hat{H}t/\hbar}\,|j_i\rangle, \tag{3.28}$$

with

$$\langle j_f|\,\varphi_f\rangle = (-2\pi\mathrm{i}\hbar)^{-\frac{1}{2}}\,\mathrm{e}^{-\mathrm{i}\varphi_f j_f/\hbar}. \tag{3.29}$$

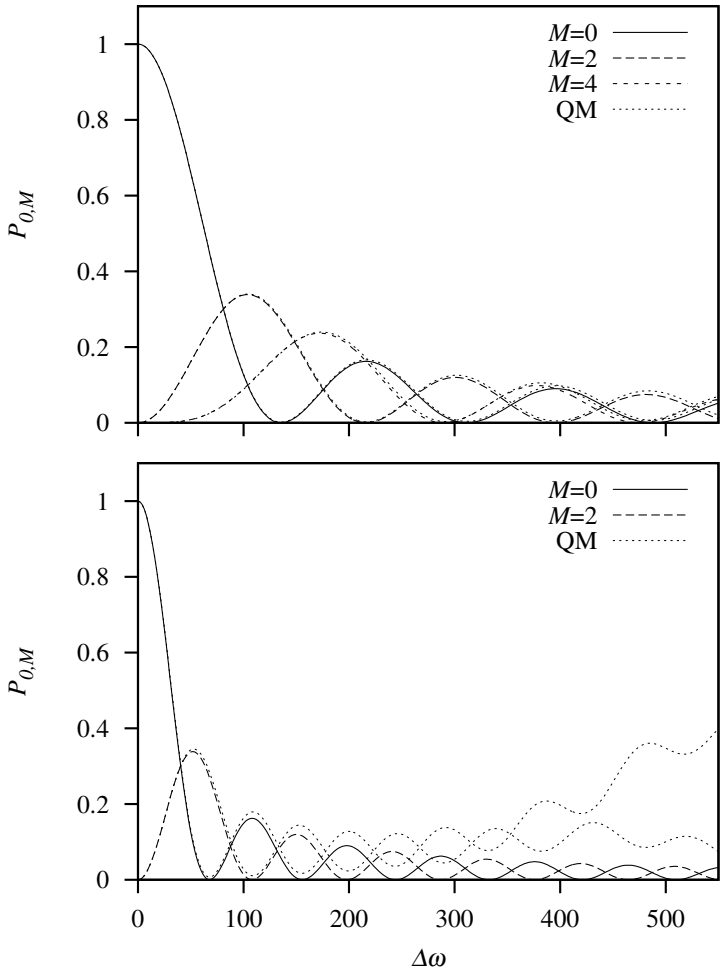

Figure 3.1: Sudden Approximation: transition probabilities for short pulses. This approximation works very well for a short pulse of width $\sigma = 0.02$ as seen in the upper panel. For $\sigma = 0.04$, lower panel, the sudden approximation begins to fail for $\Delta\omega > 200$.

Similarly the initial momentum to final coordinate amplitude is given in terms of the coordinate representation,

$$\langle\varphi_f|\,\mathrm{e}^{-\mathrm{i}\hat{H}t/\hbar}\,|j_i\rangle = \int \mathrm{d}\varphi_i\,\langle\varphi_f|\,\mathrm{e}^{-\mathrm{i}\hat{H}t/\hbar}\,|\varphi_i\rangle\,\langle\varphi_i|\,j_i\rangle, \tag{3.30}$$

with

$$\langle\varphi_i|\,j_i\rangle = (2\pi\mathrm{i}\hbar)^{-\frac{1}{2}}\,\mathrm{e}^{\mathrm{i}\varphi_i j_i/\hbar}. \tag{3.31}$$

Now it is possible to use the Van Vleck's formula [40] for the the semiclassical amplitude in coordinate representation

$$\langle\varphi_f|\,\mathrm{e}^{-\mathrm{i}\hat{H}t/\hbar}\,|\varphi_i\rangle = (2\pi\mathrm{i}\hbar)^{-\frac{1}{2}}\left|\frac{\partial^2 F_1(\varphi_f,\varphi_i;t)}{\partial\varphi_f\partial\varphi_i}\right|^{\frac{1}{2}}\exp\left[\frac{\mathrm{i}}{\hbar}F_1(\varphi_f,\varphi_i;t)\right]. \tag{3.32}$$

For a dynamical transformation this formula must be evaluated along a classical trajectory $\boldsymbol{z}_t(\boldsymbol{z}_i)$ going from $\boldsymbol{z}_i = (\varphi_i, j_i)$ at time $t = 0$ to $\boldsymbol{z}_f = (\varphi_f, j_f)$ at time t. The F_1 generating function is [60]

$$F_1(\varphi_f,\varphi_i;t) = \int_0^t \mathrm{d}t'\,[j_{t'}\dot{\varphi}_{t'} - H_{t'}], \tag{3.33}$$

for which

$$-j_i = \frac{\partial F_1(\varphi_f,\varphi_i;t)}{\partial\varphi_i}, \tag{3.34a}$$

$$j_f = \frac{\partial F_1(\varphi_f,\varphi_i;t)}{\partial\varphi_f}. \tag{3.34b}$$

The first of these equations allows to rewrite the pre-exponential function in Van Vleck's amplitude as

$$\left|\frac{\partial^2 F_1(\varphi_f,\varphi_i;t)}{\partial\varphi_f\partial\varphi_i}\right|^{\frac{1}{2}} = \left|\frac{\partial\varphi_f}{\partial j_i}\right|^{-\frac{1}{2}}. \tag{3.35}$$

Along the classical trajectory $\boldsymbol{z}_t(\boldsymbol{z}_i)$ when $\frac{\partial\varphi_f}{\partial j_i} = 0$ the trajectory encounters a caustic and Van Vleck's formula diverges. This limits Van Vleck's formula, and any semiclassical amplitude derived from it, to times before the first caustic.

Inserting (3.32) into (3.30) and evaluating the integral in the stationary phase approximation gives [41]

$$\langle \varphi_f |\, \mathrm{e}^{-\mathrm{i}\hat{H}t/\hbar}\, | j_i \rangle = (2\pi \mathrm{i}\hbar)^{-\frac{1}{2}} \left| \frac{\partial \varphi_t}{\partial \varphi_i} \right|^{-\frac{1}{2}} \exp\left[\frac{\mathrm{i}}{\hbar} F_2(\varphi_f, j_i; t) \right], \tag{3.36}$$

with the F_2 generator [20]

$$F_2(\varphi_f, j_i; t) = F_1(\varphi_f, \varphi_i; t) + j_i \varphi_i. \tag{3.37}$$

Now equation (3.33) is replaced into (3.30), which after changing integration variable to φ_i gives

$$\langle j_f |\, \mathrm{e}^{-\mathrm{i}\hat{H}t/\hbar}\, | j_i \rangle = (2\pi\hbar)^{-1} \int \mathrm{d}\varphi_i \left| \frac{\partial \varphi_t}{\partial \varphi_i} \right|^{\frac{1}{2}} \exp\left\{ \frac{\mathrm{i}}{\hbar} \left[F_2(\varphi_f, j_i; t) - \varphi_t j_f \right] \right\} \tag{3.38}$$

This is an initial value integral representation (IVR) for the semiclassical amplitude in the momentum representation. Since the modulus of the complex integrand can not diverge this formula apparently works fine at the caustics, however anytime the derivative $\frac{\partial \varphi_t}{\partial \varphi_i} = 0$ the continuity of the integrand as a function of φ_i is affected.

Evaluation of the integral (3.38) using the stationary phase approximation gives [41]

$$\langle j_f |\, \mathrm{e}^{-\mathrm{i}\hat{H}t/\hbar}\, | j_i \rangle = (2\pi\hbar)^{-\frac{1}{2}} \sum_{\varphi_i^{(r)}} \left| \frac{\partial j_t}{\partial \varphi_i} \right|^{-\frac{1}{2}} \exp\left\{ \frac{\mathrm{i}}{\hbar} F_4(j_f, j_i; t) + \mathrm{i}\frac{\pi}{4} \mathrm{sgn}\, \frac{\partial j(0^+)}{\partial \varphi_i} \right\}, \tag{3.39}$$

where the sum involves all the root trajectories with $j = j_i$ at $t = 0$ and $j = j_f$ at the final time. This semiclassical formula is limited to times before any of the trajectories crosses a momentum-space caustic $\frac{\partial j_f}{\partial \varphi_i} = 0$. The F_4 generator is given by

$$F_4(j_f, j_i; t) = \int_0^t \mathrm{d}t' \left[\varphi_{t'} \frac{\mathrm{d}j_{t'}}{\mathrm{d}t'} - H_{t'} \right], \tag{3.40}$$

and sgn is simply the sign function. The last term of the exponents requires to take the limit as t approaches zero.

3.1.7 Inclusion of Maslov Indices

Although there is a simple procedure for including the correct phase when a caustic is crossed [37, 38], this is limited to systems with one degree of freedom. The formulas quoted in this section are the one dimensional case of the general formulas found in reference [41].

To extend the validity of the semiclassical amplitudes (3.38) and (3.39) to times after the first or any later caustic it is necessary to include an extra time dependent phase, which changes only when the trajectory crosses a caustic. The time at which the k-th caustic occurs, t_k^*, is called the k-th focal time [41–43]. For the coordinate representation amplitude, equation (3.32), this extra phase was calculated originally by Maslov [77]. Following the original Maslov method, Campolieti and Brumer [41] develop similar formulas for other representations.

For the initial value integral representation amplitude (3.38) the corrected formula including Maslov's phase is

$$\langle j_f|\, \mathrm{e}^{-\mathrm{i}\hat{H}t/\hbar}\, |j_i\rangle = (2\pi\hbar)^{-1} \int \mathrm{d}\varphi_i \left|\frac{\partial\varphi_t}{\partial\varphi_i}\right|^{1/2} \mathrm{e}^{-\mathrm{i}\frac{\pi}{2}\nu(\varphi_i;t)} \exp\left\{\frac{\mathrm{i}}{\hbar}\left[F_2(\varphi_f, j_i; t) - \varphi_t j_f\right]\right\}, \tag{3.41}$$

where $\nu\left(\varphi_i; t\right)$ is the Maslov index for the initial condition φ_i at time $t_k^* < t < t_{k+1}^*$

$$\nu\left(\varphi_i; t\right) = \sum_k \left(1 - \sigma_k(\varphi_i)\right)/2, \tag{3.42}$$

with

$$\sigma_k(\varphi_i) = \lim_{\epsilon\to 0} \mathrm{sgn}\left\{\frac{\partial\varphi_{t_k^*+\epsilon}(\varphi_i, j_i)}{\partial\varphi_i}\left[\frac{\partial\varphi_{t_k^*-\epsilon}(\varphi_i, j_i)}{\partial\varphi_i}\right]^{-1}\right\}. \tag{3.43}$$

That is, the Maslov index changes after t_k^* only if $\sigma_k(\varphi_i) = -1$, *i.e.*, if $\frac{\partial\varphi_t}{\partial\varphi_i}$ is negative (positive) before t_k^* and positive (negative) after t_k^*. Since this derivative cannot diverge this is equivalent to have a trajectory crossing a caustic $\frac{\partial\varphi_t}{\partial\varphi_i} = 0$ at t_k^*.

For equation (3.39) the corrected formula is

$$\langle j_f|\, \mathrm{e}^{-\mathrm{i}\hat{H}t/\hbar}\, |j_i\rangle = (2\pi\mathrm{i}\hbar)^{-\frac{1}{2}} \sum_{\varphi_i^{(r)}} \left|\frac{\partial j_t}{\partial \varphi_i}\right|^{-\frac{1}{2}} \exp\left\{\frac{\mathrm{i}}{\hbar}F_4(j_f, j_i; t) + \mathrm{i}\frac{\pi}{2}\bar{\nu}\left(\varphi_i; t\right)\right\}, \quad (3.44)$$

with the Maslov index for the i-th root trajectory at time $t_k^* < t < t_{k+1}^*$

$$\bar{\nu}\left(\varphi_i; t\right) = -\frac{1}{2}\left[1 + \mathrm{sgn}\frac{\partial j(0^+)}{\partial \varphi_i}\right] + \sum_k \Delta\bar{\nu}_k(\varphi_i), \quad (3.45)$$

which changes across t_k by

$$\Delta\bar{\nu}_k(\varphi_i) = \lim_{\epsilon\to 0}\frac{1}{2}\left(\sigma_k - 1\right)\mathrm{sgn}\frac{\partial j_\epsilon(\varphi^*, j^*)}{\partial \varphi^*}, \quad (3.46)$$

with $\varphi^* = \varphi_{t_k^*-\epsilon}(\varphi_i, j_i)$, $j^* = j_{t_k^*-\epsilon}(\varphi_i, j_i)$, and

$$\sigma_k(\varphi_i) = \mathrm{sgn}\left\{\frac{\partial j_{t_k^*-\epsilon}(\varphi_i, j_i)}{\partial \varphi_i}\left[\frac{\partial j_{t_k^*+\epsilon}(\varphi_i, j_i)}{\partial \varphi_i}\right]^{-1}\right\}. \quad (3.47)$$

Again the Maslov index changes only if $\sigma_k(\varphi_i) = -1$, but now this change could be positive or negative depending on the sign of the partial derivative in (3.46).

3.1.8 Rotational Excitation of 2D-rotors in Laser Pulses

In practice the initial line $j_i(\varphi_i) = J_i\hbar$ is a set of phase space points homogeneously distributed along the line $j = J_i$ ($\hbar = 1$). These points are used as initial conditions in equations (3.5) which for a final time $t \gg t0$ will produce a final curve $j_f(\varphi_i)$. Since for $t \gg t_0$ the Hamiltonian is that for a free 2D-rotor these curves remains unchanged.

The use of equation (3.44) requires knowledge of all the root trajectories. For a given $j_f = J_f$ these trajectories are obtained from the curve $j_f(\varphi_i)$: the values φ_i at which $j_f(\varphi_i)$ intersects the line $j_f = J_f$ give the initial conditions of the root trajectories. These curves are shown in figure 3.2 for a pulse with $\sigma = 0.04$. As functions of the initial angle are plotted the final angle, φ_f, and the final

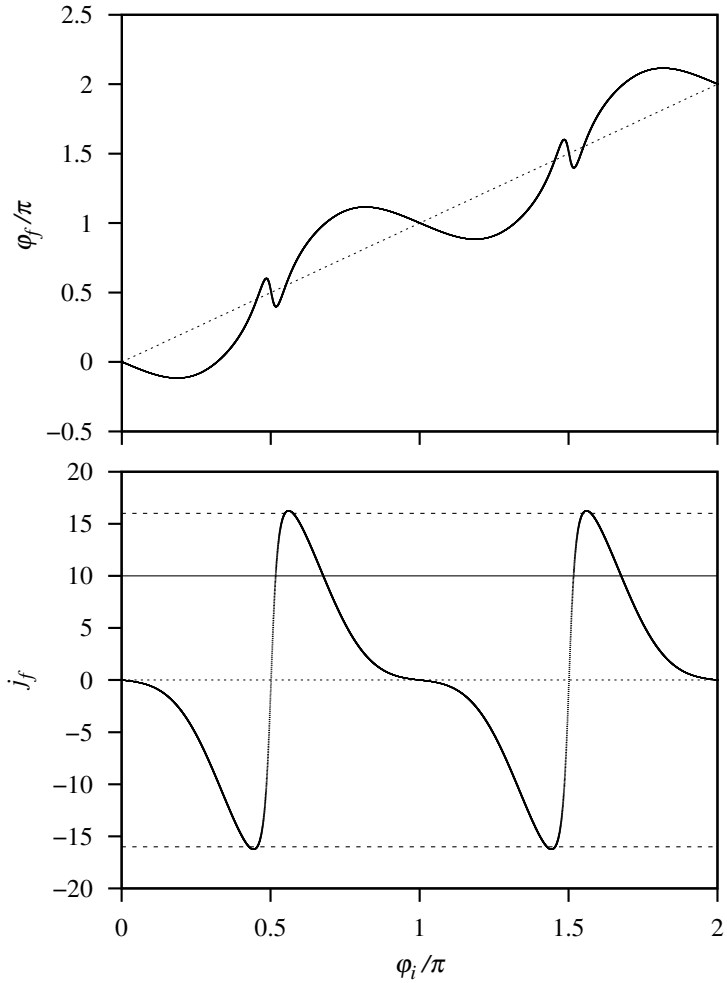

Figure 3.2: Final manifolds $\varphi_f(\varphi_i)$ and $j_f(\varphi_i)$. The initial manifolds are shown in dotted lines: the line $\varphi = \varphi_i$ for the upper panel, and $j = 0$ in the lower one. In the second panel the lines at $j = \pm 16$ are close to momentum space caustics.

action, j_f, in the upper and lower panel respectively. In both panels is seen that $\varphi_i = 0, \pi/2, \pi, 3\pi/2$ are fixed points of the equations (3.10). For $j_f(\varphi_i)$, the two dashed lines at $j_f = \pm 16$ are close to momentum space caustics, *i.e.*, the points along $j_f(\varphi_i)$ where $\frac{\partial j_f}{\partial \varphi_i} = 0$. It should be noticed also that the line $j_f = 0$ has an inflection point at $\varphi_i \approx 0, \pi$.

In the lower panel of figure 3.2 the line at $j_f = 10$ it is used to explain the methodology employed in the stationary phase approximation. As can be seen, this line intersects the final manifold in four different points giving four different values of φ_i, $\varphi_i^{(r)}$, $r \in \{1, 2, 3, 4\}$. These four intersections give the initial conditions for the root trajectories which must be used in equation (3.44). For each of the initial conditions it is necessary to obtain, at the final time, the stability matrix component $\partial j_t / \partial \varphi_i$, the accumulated value of the line integral F_4 (defined in equation (3.40)), and also the accumulated Maslov index $\bar{\nu}(\varphi_i; t)$, obtained via equations (3.45)-(3.47). For each of the root trajectories these quantities give the terms of the sum (3.44), which in general are complex quantities. Finally, adding these four complex numbers the semiclassical amplitude $\langle 10| \, \mathrm{e}^{-\mathrm{i}\hat{H}t/\hbar} \, |0\rangle$ is obtained, and from this, the transition probability $P_{0\to 10} = \left| \langle 10| \, \mathrm{e}^{-\mathrm{i}\hat{H}t/\hbar} \, |0\rangle \right|^2$.

In practice is better to interpolate the curves of final $\partial j_t / \partial \varphi_i$, F_4, and $\bar{\nu}(\varphi_i; t)$ at the root values of φ_i instead of doing the calculation over for the root trajectories alone.

The IVR transition probabilities do not require knowing the initial conditions for root trajectories but the integral (3.41) must be done. The calculation runs similarly: for all the initial conditions at the final time it is necessary to obtain the value of $\partial \varphi_t / \partial \varphi_i$, and the accumulated values of F_3 via equations (3.37) and (3.33), and the Maslov index $\nu(\varphi_i; t)$ from equations (3.42)-(3.43).

In order to compare with quantum results the classical rotational constant, $B = 1/2I$, takes the value $B = 1$. There are different types of pulses depending on σ, ranging from the short pulses with $\sigma \ll (1/B\hbar)$ to the adiabatic pulses $\sigma \gg (1/B\hbar)$ [73]. Another relevant parameter in the calculations is $\Delta\omega$ which could typically range between 0 and 800 [10].

In figure 3.3 we can see the semiclassical transition probabilities for a 2D-rotor starting at the $M = 0$ state for the case of an intense ($\Delta\omega = 400$) short pulse ($\sigma = 0.04\hbar/B$). It is clear in the figure that both semiclassical methods predict perfectly the selection rule $\Delta M = \pm 2$ for the 2D-rotor in a linearly polarized laser field, in fact this is one of the strongest features of semiclassical methods [45]. One advantage of the IVR method over stationary phase approximation is evident in the transition probabilities $P_{0\to 16}$ and $P_{0\to 0}$where the SC-SPA method fails due to the proximity of momentum caustics.

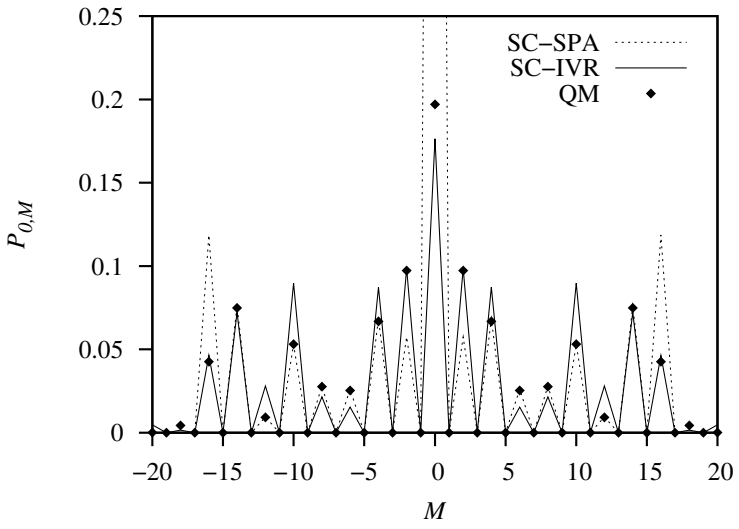

Figure 3.3: Semiclassical transition probabilities from $M = 0$ state for a 2D-rotor in an intense ($\Delta\omega = 400$) short laser pulse ($\sigma = 0.04\hbar/B$). The SC-SPA transition probabilities at $M = 0, \pm 16$ fail due to proximity to momentum caustics.

A global picture of the effect of the intense short laser on the 2D-rotor can be seen in figure 3.4 for pulses of width $\sigma = 0.04, 0.08$. In the upper panel, for $\sigma = 0.04$ it is noticed how the IVR results are in better agreement with the quantum probabilities than the sudden approximation, figure 3.1. In the same panel it is also noticed how the SPA fails completely for $\Delta\omega > 300$, surely due to the presence of momentum caustics for $j_f = 0$. For the $\sigma = 0.08$ pulse the situation gets worse for the SPA, now several caustics effect the transitions probabilities, however, the IVR results are still in good agreement with the quantum ones.

In figure 3.5 can be observed the transition probabilities $P_{0,2}$ and $P_{0,4}$ for the same pulses. In panels (a) and (b), for a pulse $\sigma = 0.04$, the two semiclassical results are in good agreement with the quantum probabilities except near $\Delta\omega = 0$ where the SPA fails. In panels (c) and (d), for $\sigma = 0.08$, it is noticed that the effect of the caustics are not as strong as in figure 3.4.

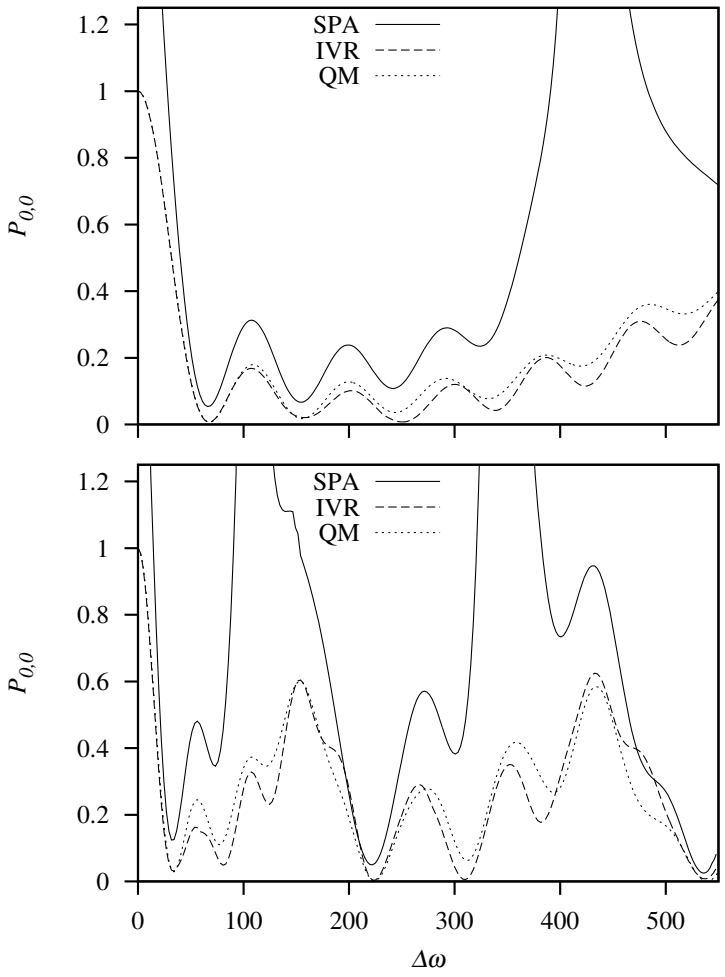

Figure 3.4: Semiclassical and quantum $P_{0\to 0}$ transition probabilities. In the upper panel a pulse of width $\sigma = 0.04$ is used, for the lower one $\sigma = 0.08$.

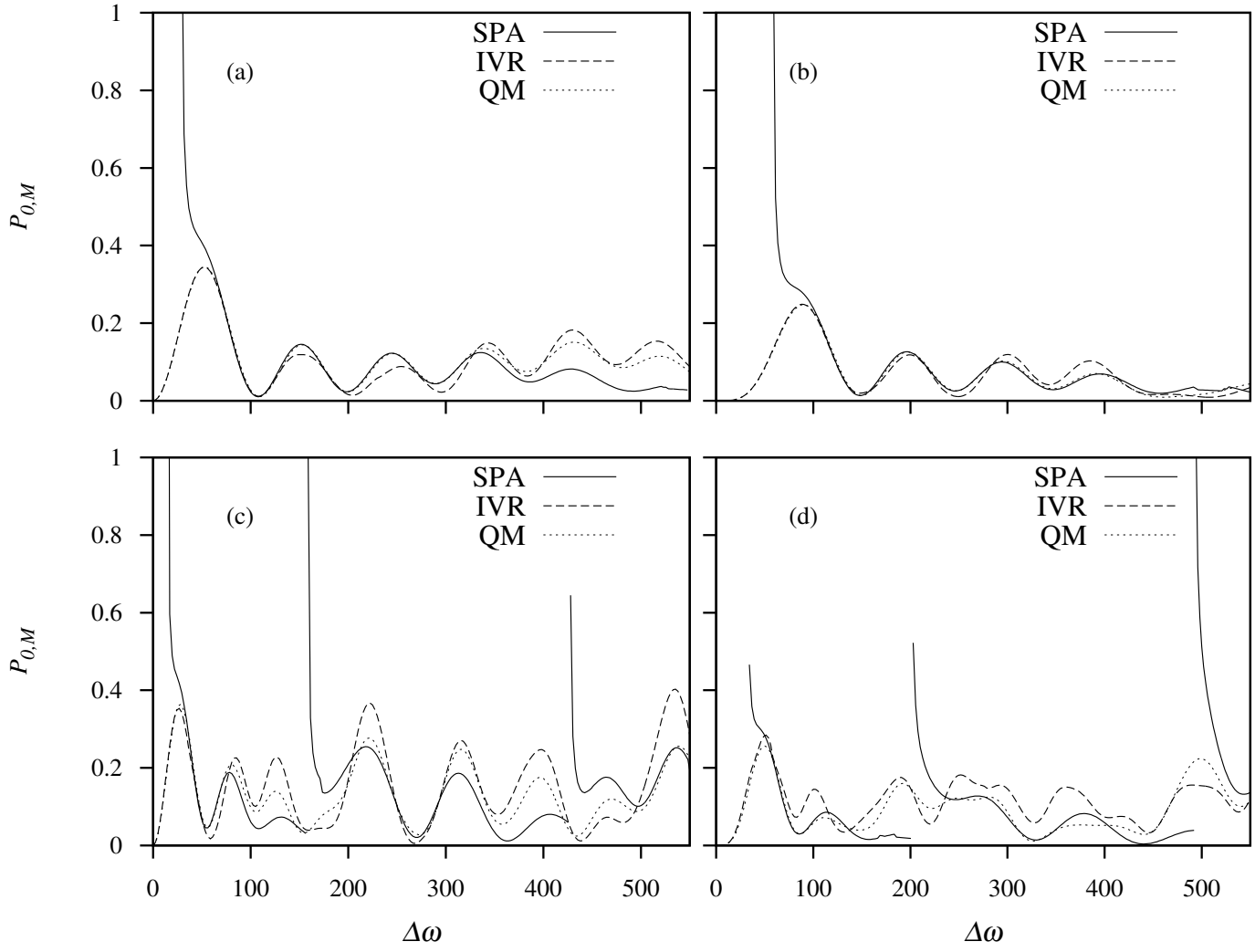

Figure 3.5: Semiclassical and quantum transition probabilities: $\sigma = 0.04$ (a) $P_{0,2}$, (b) $P_{0,4}$; $\sigma = 0.08$ (c) $P_{0,2}$, (d) $P_{0,4}$.

3.2 Semiclassical Angular Focusing of 2D-rotors

As the laser pulse reaches its maximum intensity at $t = t_0$ the potential of the rotor gets the shape of a periodic double well in the angle with maxima at $\varphi = \pi/2, 3\pi/2$ and minima at $\varphi = 0, \pi$. For an initial BS state with small quantum number M, the effect of the pulse causes a localization or focusing of trajectories near the minima of the potential energy. This focusing, among other phenomena, has been studied recently for 2D and 3D kicked rotors [78].

The stationary phase approximation for the initial momentum to final coordinate amplitude, equation (3.36), is the starting point for the semiclassical study of angular focusing. Adding the Maslov index, and considering all root trajectories this equation becomes

$$\langle\varphi_f|\, \mathrm{e}^{-\mathrm{i}\hat{H}t/\hbar}\, |j_i\rangle = (2\pi\mathrm{i}\hbar)^{-\frac{1}{2}} \sum_r \left|\frac{\partial\varphi_t}{\partial\varphi_i}\right|^{-\frac{1}{2}} \exp\left[\frac{\mathrm{i}}{\hbar}F_2(\varphi_f, j_i; t) - \mathrm{i}\frac{\pi}{2}\nu(\varphi_i; t)\right], \quad (3.48)$$

with $\nu(\varphi_i, t)$ given by equations (3.42) and (3.43).

The initial state is a line of initial conditions with constant $j_i = J_i\hbar$ and $0 < \varphi_i < 2\pi$. This initial manifold is propagated classically and after the effect of the pulse, at time $t = t_f$, the curve $\varphi_f(\varphi_i)$ is used to get the root trajectories. The intersections of the curve $\varphi_f(\varphi_i)$ with a line of constant φ_f give the root trajectories for that value of φ_f. Using equation (3.48) for all possible φ_f is obtained the semiclassical final wave function for the initial state with $j_i = J_i\hbar$. The probability density of finding the rotor at certain value of the angle after the effect of the pulse is given by

$$P(\varphi) = \left|\langle\varphi|\, \mathrm{e}^{-\mathrm{i}\hat{H}t/\hbar}\, |j_i\rangle\right|^2. \quad (3.49)$$

In figure 3.6 can be seen the probability density for a pulse with $\Delta\omega = 400$, $\sigma = 0.04\hbar/B$. The center of the Gaussian profile is at $t = 10\sigma$. Although this

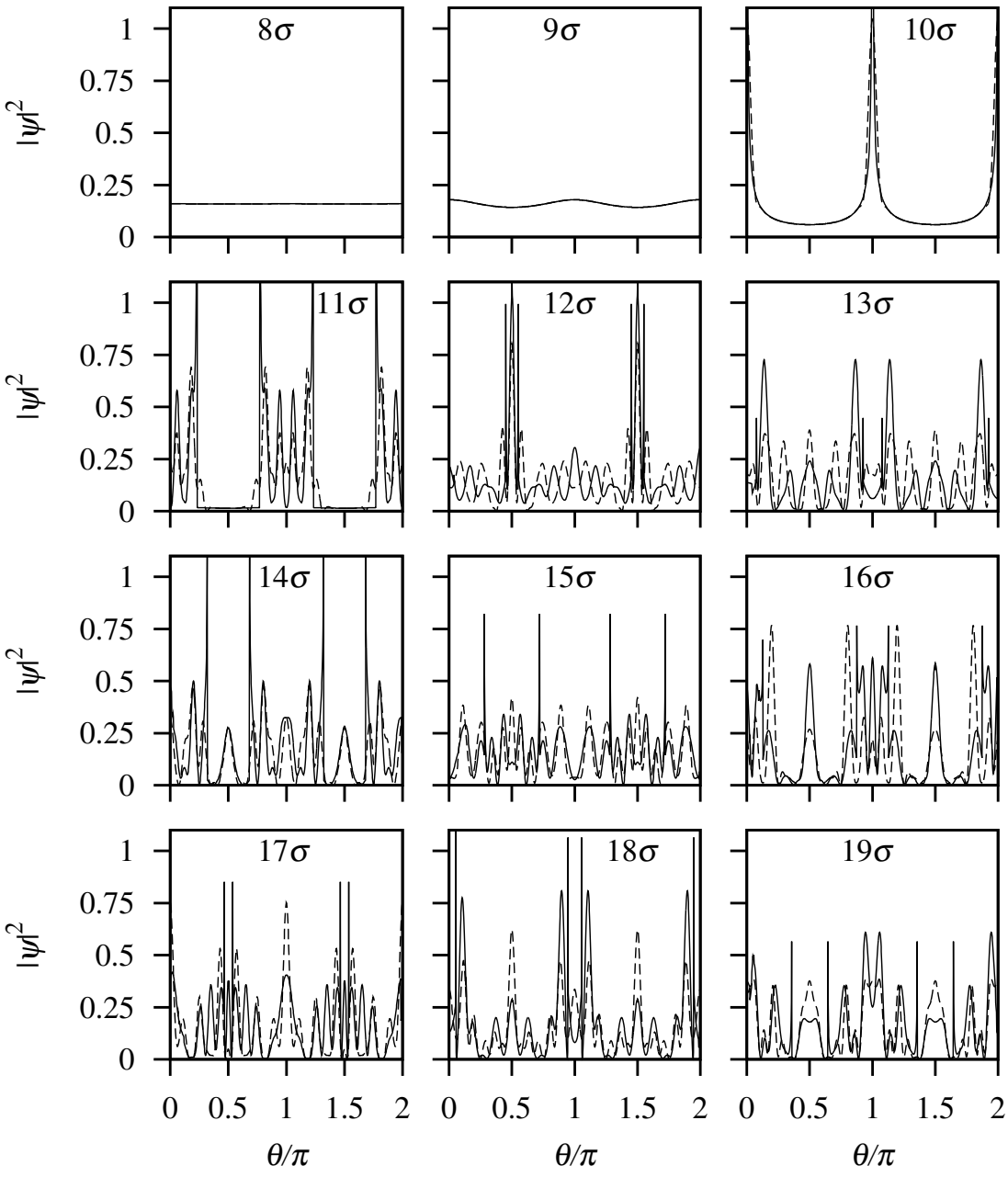

Figure 3.6: Semiclassical (solid) and quantum (dashed) probability densities. A pulse with $\Delta\omega = 400$, $\sigma = 0.04\hbar/B$. The legend inside each panel indicates the elapsed time, the center of the pulse is at 10σ.

is a simple Van Vleck semiclassical propagation the agreement with the quantum results [72] is qualitatively acceptable.

3.3 Semiclassical Propagation Using the Herman-Kluk IVR

In this section the Herman-Kluk (HK) propagator is used to study the rotational dynamics and spectrum of 2D and 3D rotors in combined electric and laser fields. Although the HK propagator is applicable only to cartesian degrees of freedom several schemes and approximations have been develop to deal with rotational degrees of freedom [48, 49].

The Herman-Kluk (HK) or harmonic oscillator coherent states (HOCS) IVR is one of the most popular method to propagate wave functions semiclassically. This method is based in the frozen Gaussian approximation [46, 47, 54], in which the center of a HOCS follows a classical trajectory in phase space without changing its initial Gaussian shape. The initial wave function is represented in terms of these coherent states as an initial value integral, and the propagation of each of these Gaussians contribute to the final wave function.

In the coordinate representation a HOCS centered at $z_t = (q_t, p_t)$ can be written as

$$\langle q|z_t\rangle = \left(\frac{\gamma}{\pi}\right)^{1/4} \exp\left\{-\frac{\gamma}{2}\left(q-q_t\right)^2 + \frac{\mathrm{i}}{\hbar}p_t\left(q-q_t\right)\right\}, \tag{3.50}$$

where γ is a parameter controlling the width of the coherent state in the coordinate (momentum) direction, and z_t is the position at time t of a phase space trajectory

starting at $z_0 = (q_0, p_0)$ at time $t = 0$,

$$\begin{aligned} z_t &= z(z_0, t) \\ &= (q_t, p_t) \\ &= (q(q_0, p_0, t), p(q_0, p_0, t)). \end{aligned} \tag{3.51}$$

The HK semiclassical amplitude connecting the positions q' and q'' at times 0 and t respectively, $K(q'', t; q', 0)$, is commonly expressed in the form

$$K(q'', t; q', 0) = \frac{1}{2\pi\hbar} \int \mathrm{d}z_0 \, \langle q''|z_t\rangle \, C_t(z_0) \mathrm{e}^{\frac{\mathrm{i}}{\hbar} S_t(z_0)} \, \langle z_0|q'\rangle \, . \tag{3.52}$$

The integral is taken over the whole phase space of the system, which for a cartesian degree of freedom means $\mathbb{R}^2$. The $C_t(z_0)$ is commonly called HK prefactor and has the form

$$C_t(z_0) = \left[\frac{1}{2}\left(\frac{\partial q_t}{\partial q_0} + \frac{\partial p_t}{\partial p_0} - \mathrm{i}\gamma\hbar\frac{\partial q_t}{\partial p_0} + \frac{\mathrm{i}}{\gamma\hbar}\frac{\partial p_t}{\partial q_0}\right)\right]^{1/2} . \tag{3.53}$$

Finally, $S_t(z_0)$ is the classical action [60], an F_1 generator [20],

$$S_t(z_0) = \int_0^t \mathrm{d}t' \, (p_{t'}\dot{q}_{t'} - H) \, , \tag{3.54}$$

with H as the Hamiltonian of the system.

The partial derivatives in the HK prefactor are the components of the Jacobian matrix for the canonical transformation $z_t = z(z_0, t)$ [60], *i.e.*, the stability matrix, appendix C.

For an initial wave function $\psi(q, 0) = \langle q|\psi_0\rangle$, the semiclassical HK evolved wave function at time t, $\psi(q, t) = \langle q|\psi_t\rangle$ is

$$\begin{aligned} \langle q|\psi_t\rangle &= \int_{\mathbb{R}} \mathrm{d}q' K(q, t; q', 0) \, \langle q'|\psi_0\rangle \\ &= \frac{1}{2\pi\hbar} \int \mathrm{d}z_0 \, \langle q|z_t\rangle \, C_t(z_0) \mathrm{e}^{\frac{\mathrm{i}}{\hbar} S_t(z_0)} \, \langle z_0|\psi_0\rangle \, . \end{aligned} \tag{3.55}$$

This integral can be evaluated as a time dependent average over the initial phase space with statistical weight given by $|\langle z_0|\psi_0\rangle|$ [47, 50].

3.4 HK Method for Periodic Potentials

The phase space for a 2D rotor is the cartesian product $[0, 2\pi) \times \mathbb{R}$. Since this is not $\mathbb{R}^2$, HK cannot be applied directly. The 2π periodicity of the angle variable is not compatible with the HOCS, except as an approximation, in the case of very narrow Gaussians in configuration space (large γ). In the angle representation a periodic coherent state, $\langle\phi|\phi', j'\rangle$, can be defined in terms of HOCS

$$\begin{aligned} \langle\phi|\phi', j'\rangle &\equiv \sum_{n\in\mathbb{Z}} \langle\phi|\phi' + 2n\pi, j'\rangle \\ &= \sum_{n\in\mathbb{Z}} \langle\phi + 2n\pi|\phi' j'\rangle \,, \end{aligned} \tag{3.56}$$

with the angles $\phi, \phi' \in [0, 2\pi)$.

The unit operator for the real line $\mathbb{R}$,

$$\hat{1} = \int_{\mathbb{R}} \mathrm{d}q \, |q\rangle \langle q| \,, \tag{3.57}$$

can be expressed in terms of the unit operator on the circle $\mathbb{S}^1$, $\hat{1}_{\mathbb{S}^1} = \int_0^{2\pi} \mathrm{d}\phi \, |\phi\rangle \langle\phi|$, as

$$\hat{1} = \sum_{n\in\mathbb{Z}} \int_0^{2\pi} \mathrm{d}\phi \, |\phi + 2n\pi\rangle \langle\phi + 2n\pi| \,. \tag{3.58}$$

The product of two periodic coherent states can be written in terms of HOCS with the use of $\hat{1}_{\mathbb{S}^1}$,

$$\begin{aligned} (\phi'' j''|\phi' j') &= \int_0^{2\pi} \mathrm{d}\phi \, (\phi'' j''|\phi\rangle \langle\phi|\phi' j') \\ &= \sum_{m,n\in\mathbb{Z}} \int_0^{2\pi} \mathrm{d}\phi \, \langle\phi'' j''|\phi + 2n\pi\rangle \langle\phi + 2m\pi|\phi' j'\rangle \,, \end{aligned} \tag{3.59}$$

which after some manipulations of the summation indices can be written

$$\begin{aligned} (\phi'' j''|\phi' j') &= \sum_{n\in\mathbb{Z}} \int_{\mathbb{R}} \mathrm{d}q \, \langle\phi'' j''|q\rangle \langle q|\phi' + 2n\pi, j'\rangle \\ &= \sum_{n\in\mathbb{Z}} \int_{\mathbb{R}} \mathrm{d}q \, \langle\phi'' + 2n\pi, j''|q\rangle \langle q|\phi' j'\rangle \,. \end{aligned} \tag{3.60}$$

Using the expression for the coordinate representation of a HOCS, equation (3.50), the integral can be solved to get

$$(\phi'' j''|\phi' j') = \exp\left[-\frac{\gamma}{4}\Delta\phi^2 - \frac{1}{4\gamma\hbar^2}\Delta j^2 + \frac{\mathrm{i}}{2\hbar}\left(j'' + j'\right)\Delta\phi\right]\vartheta_3\left(\eta,\zeta\right), \tag{3.61}$$

where $\Delta\phi = \phi'' - \phi'$, $\Delta j = j'' - j'$, and the third Jacobian elliptic theta function [79] (appendix D), $\vartheta_3\left(\eta,\zeta\right)$, is given by

$$\vartheta_3\left(\eta,\zeta\right) = \sum_{n\in\mathbb{Z}} \eta^{n^2} \mathrm{e}^{2\mathrm{i}n\zeta}, \tag{3.62}$$

with the nome η, and ζ obtained from

$$\eta = \exp\left\{-\gamma\pi^2\right\}, \tag{3.63a}$$

$$\zeta = \frac{\pi}{2\hbar}\left[\left(j'' + j'\right) + \mathrm{i}\gamma\hbar\left(\phi'' - \phi'\right)\right]. \tag{3.63b}$$

The HK semiclassical amplitude on $\mathbb{S}^1$, $K_{\mathbb{S}^1}\left(\phi'', t; \phi', 0\right)$, connecting ϕ'' at time t with ϕ' at time 0, can be expressed in terms of the HK amplitude on $\mathbb{R}^1$, equation (3.52), by

$$K_{\mathbb{S}^1}\left(\phi'', t; \phi', 0\right) = \sum_{n\in\mathbb{Z}} K\left(\phi'' + 2n\pi, t; \phi', 0\right). \tag{3.64}$$

Using (3.52) and (3.58) in equation (3.64) and after some work,

$$K_{\mathbb{S}^1}\left(\phi'', t; \phi', 0\right) = \frac{1}{2\pi\hbar}\int_0^{2\pi} \mathrm{d}\phi_0 \int_{\mathbb{R}} \mathrm{d}j_0 \left\langle \phi''|\phi_t j_t\right\rangle C_t\left(\phi_0 j_0\right) \mathrm{e}^{\frac{\mathrm{i}}{\hbar}S_t(\phi_0 j_0)} \left(\phi_0 j_0|\phi'\right\rangle. \tag{3.65}$$

gives the HK amplitude on $\mathbb{S}^1$ in terms of periodic coherent states. Writing this amplitude in terms of the time evolution operator $U_{HK}(t)$

$$K_{\mathbb{S}^1}\left(\phi'', t; \phi', 0\right) = \left\langle \phi''\right| U_{HK}(t, 0) \left|\phi'\right\rangle, \tag{3.66}$$

with the HK propagator, $U_{HK}(t)$, given by

$$U_{HK}(t, 0) = \frac{1}{2\pi\hbar}\int_0^{2\pi} \mathrm{d}\phi_0 \int_{\mathbb{R}} \mathrm{d}j_0 \left|\phi_t j_t\right\rangle C_t\left(\phi_0 j_0\right) \mathrm{e}^{\frac{\mathrm{i}}{\hbar}S_t(\phi_0 j_0)} \left(\phi_0 j_0\right|. \tag{3.67}$$

3.4.1 Application: Energy Spectrum of the Particle on a Ring

The spectrum of the 2D rotor has been obtained semiclassically using Gaussian wave packets dynamics [80]. In this section the HK propagator is used to get analytically the spectrum of the 2D-rotor. The Hamiltonian for the particle on a ring is,

$$H = Bj^2. \tag{3.68}$$

The conjugate variable ϕ does not appear in H, and j is a constant of motion. From Hamilton's equations:

$$\frac{\mathrm{d}\phi}{\mathrm{d}t} = 2Bj, \qquad \frac{\mathrm{d}j}{\mathrm{d}t} = 0; \tag{3.69}$$

it is possible to obtain the trajectory as a function of the initial conditions ϕ_0 and j_0

$$j_t = j_0, \qquad \phi_t = \phi_0 + 2Bj_0t. \tag{3.70}$$

Following the results in appendix C, the monodromy matrix is given by

$$\mathsf{M}(t) = \begin{pmatrix} 1 & 2Bt \\ 0 & 1 \end{pmatrix}, \tag{3.71}$$

which, after replacing into (3.53), gives the HK prefactor

$$C_t = (1 - \mathrm{i}\gamma\hbar Bt)^{1/2}. \tag{3.72}$$

The action is obtained combining (3.69) and (3.70) into equation (3.54) to get after integration

$$S_t(j_0) = Bj_0^2t. \tag{3.73}$$

Using the eigenstates of the particle on a ring, $|m\rangle$, the HK semiclassical autocorrelation function is

$$\begin{aligned} A_m(t) &= \int_0^{2\pi} \mathrm{d}\phi'' \int_0^{2\pi} \mathrm{d}\phi' \, \langle m|\phi''\rangle \, K_{\mathbb{S}^1}\left(\phi'', t; \phi', 0\right) \langle \phi'|m\rangle \\ &= \frac{1}{2\pi\hbar} \int_0^{2\pi} \mathrm{d}\phi_0 \int_{\mathbb{R}} \mathrm{d}j_0 \, \langle m|\phi_t j_t\rangle \, C_t\left(\phi_0 j_0\right) \mathrm{e}^{\frac{\mathrm{i}}{\hbar} S_t(\phi_0 j_0)} \left(\phi_0 j_0|m\right\rangle . \end{aligned} \tag{3.74}$$

The product of a periodic coherent state and an eigenvector $|m\rangle$ is

$$\begin{aligned} (\phi j|m\rangle &= \sum_{n\in\mathbb{Z}} \langle \phi + 2n\pi, j|m\rangle \\ &= \sum_{n\in\mathbb{Z}} \int_0^{2\pi} \mathrm{d}\phi' \, \langle \phi j|\phi' + 2n\pi\rangle \, \langle \phi' + 2n\pi|m\rangle \\ &= \int_{\mathbb{R}} \mathrm{d}q \, \langle \phi j|q\rangle \, \langle q|m\rangle . \end{aligned} \tag{3.75}$$

where $\hat{1}_{\mathbb{S}^1}$, the periodicity of $\langle \phi|m\rangle = \left(1/\sqrt{2\pi}\right) \mathrm{e}^{\mathrm{i}m\phi}$, and equation (3.58) have been used. Finally, performing the overlap integral casts

$$(\phi j|m\rangle = \left(\frac{1}{\gamma\pi}\right)^{1/4} \exp\left[-\frac{1}{2\gamma\hbar^2}\left(j - m\hbar\right)^2 + \mathrm{i}m\phi\right]. \tag{3.76}$$

All the pieces are ready and the initial value integral (3.74) can be performed with some work to get

$$A_m(t) = \exp\left(-\mathrm{i}\hbar B m^2 t\right). \tag{3.77}$$

The energy spectrum is obtained after taking the Fourier transform of $A_m(t)$ [81, 82]

$$\begin{aligned} \bar{A}_m(E) &= \frac{1}{\sqrt{2\pi\hbar}} \int_{\mathbb{R}} \mathrm{d}t \mathrm{e}^{\mathrm{i}Et/\hbar} A_m(t) \\ &= \frac{1}{\sqrt{2\pi\hbar}} \int_{\mathbb{R}} \mathrm{d}t \exp\left\{(\mathrm{i}/\hbar)\left[E - \hbar^2 B m^2\right] t\right\} \\ &= \sqrt{2\pi\hbar}\, \delta(E - \hbar^2 B m^2), \end{aligned} \tag{3.78}$$

which is no zero only for

$$E = B\hbar^2 m^2, \tag{3.79}$$

the exact levels for the particle on a ring, equation (3.15).

3.4.2 Energy Spectrum of a 2D-rotor in Electric Fields

This problem has been already treated within the HK approach to obtain autocorrelation functions and comparing with quasiclassical and quantum results [49]. Here we extend further this treatment to get the energy spectrum of a 2D rotor in static fields.

In terms of action-angle variables, the Hamiltonian of a 2D rotor in a static electric field is

$$H = Bj^2 - \omega \cos q_j, \tag{3.80}$$

where $\omega = d_0 \varepsilon_S$ gives the magnitude of interaction between the rotor and the field. Hamilton's equation's of motion are

$$\frac{\mathrm{d}q_j}{\mathrm{d}t} = 2Bj, \tag{3.81a}$$

$$\frac{\mathrm{d}j}{\mathrm{d}t} = -\omega \sin q_j. \tag{3.81b}$$

The classical trajectory is $z_t = (q_{j,t}, j_t)$. In these terms, the Hessian matrix for the Hamiltonian (3.80) is given by

$$\mathsf{H}_{z,z}(t) = \frac{\partial^2 H}{\partial z^2} = \begin{pmatrix} \omega \cos q_{j,t} & 0 \\ 0 & 2B \end{pmatrix}. \tag{3.82}$$

This matrix is needed to get the stability matrix through the relation,

$$\dot{\mathsf{M}}(t) = \mathsf{J}\mathsf{H}_{z,z}(t)\mathsf{M}(t), \tag{3.83}$$

where J represents the symplectic matrix, appendix C. With the stability matrix the HK prefactor is calculated taking care of its continuity on the complex plane.

The autocorrelation function is obtained using equations (3.74)-(3.76). For the initial states $|\psi(0)\rangle = \langle\phi|m\rangle$ (for $m = 0, 1$) we obtained A_0 and A_1, which are

shown in figure 3.7 for $\omega = 40$, $B = 1$. Observe how HK follows the quantum propagation very well for $t < 1$, and with qualitative good agreement for $t > 1$. From these autocorrelation functions the energy spectra $\bar{A}_0$ and $\bar{A}_1$ are obtained after Fourier transform, equation (3.78). In figure 3.8 the spectra for figure 3.7 are shown. The even (odd) state, $m = 0$ ($m = 1$), generates mostly the even (odd) energy peaks. The semiclassical spectrum is in excellent agreement with the quantum eigenvalues, except close to the potential energy barrier at $q_j = \pi$. This is a failure of the HK method that have been already noticed for systems with potential energy barriers and specifically for a periodic potential [49].

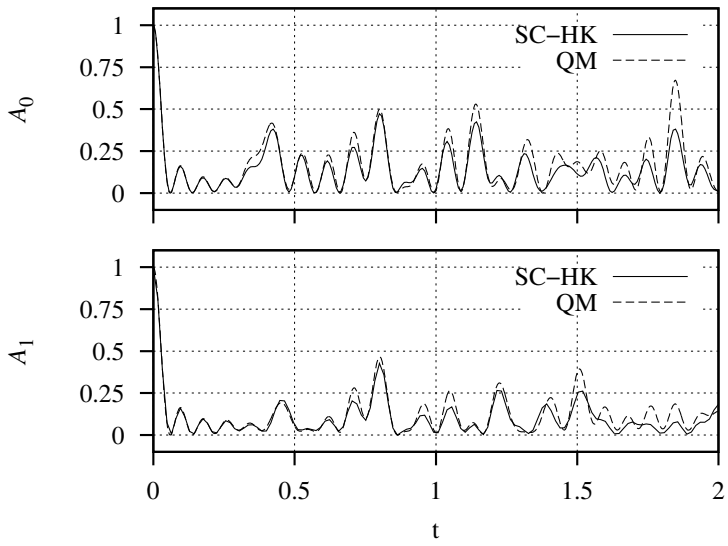

Figure 3.7: Semiclassical and quantum autocorrelation function for a 2D rotor in a static field, $\omega = 40$, $B = 1$. The upper panel shows A_0, for initial state with $m = 0$. In the lower panel the initial state is $m = 1$.

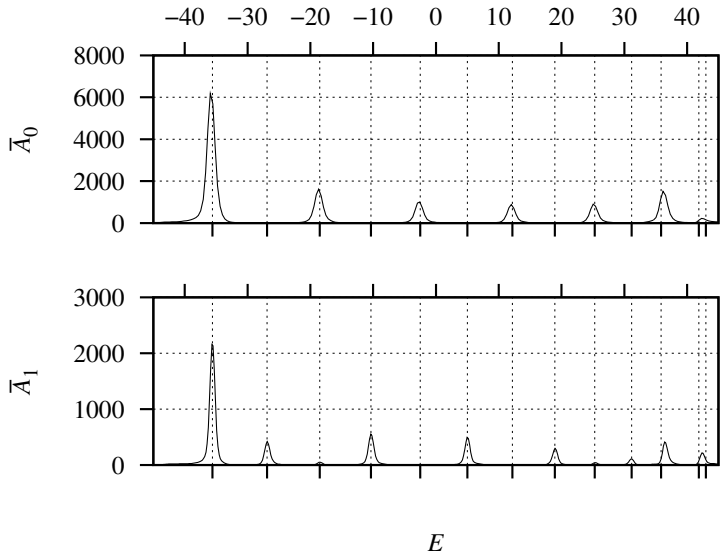

Figure 3.8: Semiclassical energy spectrum for a 2D rotor in a static field, $\omega = 40$, $B = 1$. The vertical grid lines are set at the quantum energy levels. The upper panel shows the spectrum for initial state $m = 0$, the lower one for $m = 1$.

3.5 Alignment and Orientation of a 2D-Rotor in Electric Fields

Orientation and alignment can be obtained easily in the framework of Quantum Mechanics [72, 83]. In this section we obtain semiclassical formulas for orientation and alignment.

For the state $|\psi(t)\rangle$ the orientation and alignment of a 2D rotor are given by the average of $\cos q_j$ and $\cos^2 q_j$ respectively

$$\langle \cos q_j \rangle_\psi (t) = \langle \psi(t)| \cos q_j |\psi(t)\rangle \,, \tag{3.84a}$$

$$\left\langle \cos^2 q_j \right\rangle_\psi (t) = \langle \psi(t)| \cos^2 q_j |\psi(t)\rangle \,. \tag{3.84b}$$

If the initial state is a periodic coherent state $|\psi(0)\rangle = |z_0)$, semiclassically the wave function at time t is $|\psi(t)\rangle = U_{HK}(t,0)\,|z_0)$, with $|z_0) \equiv |j_0\phi_0)$. Using equation (3.67) the orientation (α=1) and alignment (α=2) are given by the double phase

space integral

$$\begin{aligned}\left\langle \cos^{\alpha} q_j \right\rangle_{\psi}(t) &= \left(z_0\right| U_{HK}^{\dagger}(t,0)\cos^{\alpha} q_j U_{HK}(t,0)\left|z_0\right) \\ &= \frac{1}{(2\pi\hbar)^2}\int_0^{2\pi}\mathrm{d}\phi_0''\int_{\mathbb{R}}\mathrm{d}j_0''\int_0^{2\pi}\mathrm{d}\phi_0'\int_{\mathbb{R}}\mathrm{d}j_0' f(t;z_0,z_0',z_0''),\end{aligned} \tag{3.85}$$

with

$$f(t;z_0,z_0',z_0'') = \left(z_0|z_0''\right)\left(z_0'|z_0\right) C_t(z_0'')^* C_t(z_0')\mathrm{e}^{\frac{\mathrm{i}}{\hbar}\left[S_t(z_0')-S_t(z_0'')\right]}\left(z_t''\right|\cos^{\alpha}\phi\left|z_t'\right). \tag{3.86}$$

For the last term in (3.86) it is obtained (see Appendix E)

$$\left(z_t''\right|\cos\phi\left|z_t'\right) = \mathrm{e}^{-1/4\gamma}\frac{\vartheta_4(\eta,\zeta)}{\vartheta_3(\eta,\zeta)}\left(z_t''|z_t'\right)\cosh\left(\frac{\Delta j}{2\gamma\hbar}+\mathrm{i}\bar{\phi}\right), \tag{3.87a}$$

$$\left(z_t''\right|\cos^2\phi\left|z_t'\right) = \frac{\left(z_t''|z_t'\right)}{2}\left[1+\mathrm{e}^{-1/\gamma}\cosh\left(\frac{\Delta j}{\gamma\hbar}+2\mathrm{i}\bar{\phi}\right)\right], \tag{3.87b}$$

where $\bar{\phi} = (\phi_t'+\phi_t'')/2$, $\bar{j} = (j_t'+j_t'')/2$, $\Delta\phi = \phi_t''-\phi_t'$, and $\Delta j = j_t''-j_t'$. The n-th Jacobian elliptic theta function $\vartheta_n(\eta,\zeta)$ is defined in terms of

$$\eta = \mathrm{e}^{-\gamma\pi^2}, \tag{3.88a}$$

$$\zeta = \frac{\pi}{2\hbar}\left[2\bar{j}+\mathrm{i}\hbar\gamma\Delta\phi\right]. \tag{3.88b}$$

For large values of γ, $\eta \approx 0$, and $\vartheta_n(0,\zeta) \approx 1$. Equations (3.87) can be approximated as

$$\left(z_t''\right|\cos\phi\left|z_t'\right) = \left(z_t''|z_t'\right)\cos\bar{\phi}, \tag{3.89a}$$

$$\left(z_t''\right|\cos^2\phi\left|z_t'\right) = \left(z_t''|z_t'\right)\cos^2\bar{\phi}, \tag{3.89b}$$

where the identities $\cosh \mathrm{i}\phi = \cos\phi$, and $2\cos^2\phi = 1+\cos 2\phi$ have been used.

For a periodic coherent state with $\gamma = 10$, equations (3.85)-(3.87) were used to calculate the orientation, $\langle\cos q_j\rangle$, and the alignment, $\langle\cos^2 q_j\rangle$, in figures 3.9 and 3.10 for a 2D-rotor in static fields of strength $\omega = 40$ and $\omega = 120$, respectively. The time is measured in rotational periods, the quantum results were obtained using

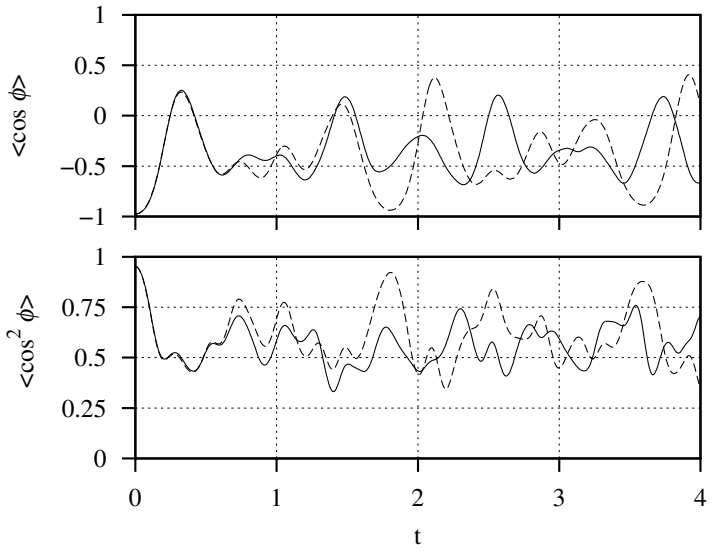

Figure 3.9: Orientation, $\langle \cos q_j \rangle$, and alignment, $\langle \cos^2 q_j \rangle$, for a 2D-rotor in a $\omega = 40$ static field. Quantum results in dashed line.

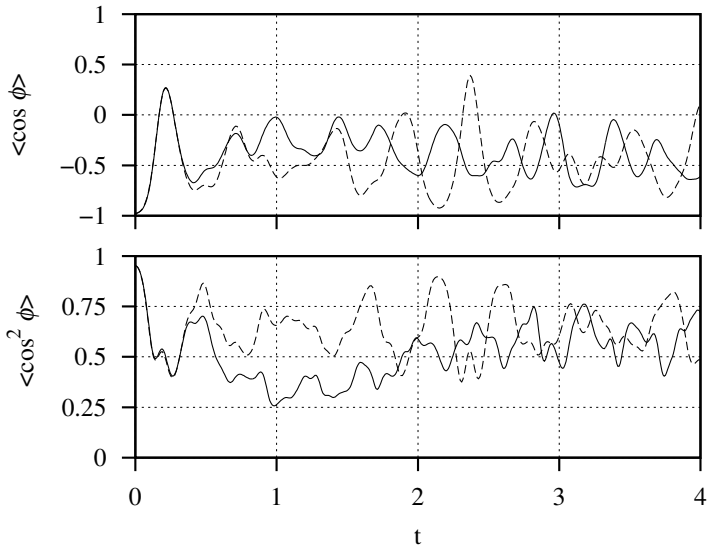

Figure 3.10: Orientation, $\langle \cos q_j \rangle$, and alignment, $\langle \cos^2 q_j \rangle$, for a 2D-rotor in a $\omega = 120$ static field. Quantum results in dashed line.

symplectic propagators for the Schrödinger equation [72]. For $\omega = 40$ the SC-HK result is practically exact for short times, and makes a good agreement before the second rotational period, and keeps qualitatively fine for longer times. In figure 3.10 the orientation shows a good behavior for times before the first rotational period and it is fine for longer times, the alignment presents good agreement only at short times. These results were obtained employing Monte-Carlo methods [84,85] for the evaluation of the 4-dimensional integrals (3.85). A total of 5×10^5 trajectories were used in the Gaussian sampling of initial conditions.

3.6 Semiclassical HK Energy Spectrum for a 3D-Rotor in Tilted Fields

The implementation of the HK method for rotational degrees of freedom has been dealt before to study the tunneling dynamics of the HCl dimer [48], and the water bender [86]. In this approach the HK coherent state scheme is employed to propagate an initial wave function, and to get the autocorrelation function and the spectrum. The HK implementation for 2D rotors required of the definition of periodic coherent states (for large γ) and the development of a suitable propagator. This is not the approach followed for the 3D rotor. Instead of defining periodic coherent, standard HOCS are defined in terms of the spherical polar angles θ and ϕ.

In analogy with the cartesian problem, in coordinate representation, a coherent

state with center at $\boldsymbol{z}' = (\theta'\phi' p'_\theta p'_\phi)$ is given by the product

$$\begin{aligned}\langle\theta\phi|\boldsymbol{z}'\rangle &= \left\langle\theta\phi|\theta'\phi' p'_\theta p'_\phi\right\rangle \\ &= \langle\theta|\theta' p'_\theta\rangle \left\langle\phi|\phi' p'_\phi\right\rangle \\ &= \left(\frac{\gamma}{\pi}\right)^{\frac{1}{2}} \exp\left\{-\frac{\gamma}{2}\left[(\theta-\theta')^2 + (\phi-\phi')^2\right] + \frac{\mathrm{i}}{\hbar}\left[p'_\theta\left(\theta-\theta'\right) + p'_\phi\left(\phi-\phi'\right)\right]\right\},\end{aligned} \tag{3.90}$$

where, for the sake of simplicity, the subindex t indicating the time dependence is omitted.

The autocorrelation function for a given wave function $\Psi(\theta, \phi, t)$ is given by

$$\begin{aligned}A_\Psi(t) &= \langle\Psi(0)|\Psi(t)\rangle \\ &= \frac{1}{4\pi^2\hbar^2}\int \mathrm{d}z_0 \left\langle\Psi_i|z_t\right\rangle C_t(z_0)\mathrm{e}^{\frac{\mathrm{i}}{\hbar}S_t(z_0)}\left\langle z_0|\Psi_i\right\rangle,\end{aligned} \tag{3.91}$$

where $\Psi_i = \Psi(0)$. The initial wave function employed is a coherent state centered at $\boldsymbol{z}_i = (\theta_i, \phi_i, p_{\theta,i}, p_{\phi,i})$

$$\langle\theta\phi|\Psi_i\rangle = \langle\theta|\psi_{\theta,i}\rangle\langle\phi|\psi_{\phi,i}\rangle, \tag{3.92}$$

with

$$\langle\theta|\psi_{\theta,i}\rangle = \left(\frac{\gamma_\theta}{\pi}\right)^{\frac{1}{4}} \exp\left\{-\frac{\gamma_\theta}{2}\left(\theta-\theta_i\right)^2 + \frac{\mathrm{i}}{\hbar}p_{\theta,i}\left(\theta-\theta_i\right)\right\}, \tag{3.93a}$$

$$\langle\phi|\psi_{\phi,i}\rangle = \left(\frac{\gamma_\phi}{\pi}\right)^{\frac{1}{4}} \exp\left\{-\frac{\gamma_\phi}{2}\left(\phi-\phi_i\right)^2 + \frac{\mathrm{i}}{\hbar}p_{\phi,i}\left(\phi-\phi_i\right)\right\}. \tag{3.93b}$$

The overlap of the coherent state (3.90) with the initial wavefunction (3.92) is given by

$$\begin{aligned}\langle\boldsymbol{z}'|\Psi_i\rangle &= \int_0^\pi \mathrm{d}\theta\sin\theta\int_0^{2\pi}\mathrm{d}\phi\left\langle\boldsymbol{z}'|\theta\phi\right\rangle\langle\theta\phi|\Psi_i\rangle \\ &= \int_0^\pi \mathrm{d}\theta\sin\theta\left\langle\theta' p'_\theta|\theta\right\rangle\langle\theta|\psi_{\theta,i}\rangle\int_0^{2\pi}\mathrm{d}\phi\left\langle\phi' p'_\phi|\phi\right\rangle\langle\phi|\psi_{\phi,i}\rangle.\end{aligned} \tag{3.94}$$

If the coherent state, and the initial wave function, are highly localized in configuration space (large γ's), the extension of the integration domain to $\mathbb{R}^2$ could be

a good approximation,

$$\langle \boldsymbol{z}'|\Psi_i\rangle \approx \int_{\mathbb{R}} \mathrm{d}\theta \sin\theta \,\langle \theta' p'_\theta|\theta\rangle \,\langle \theta|\psi_{\theta,i}\rangle \int_{\mathbb{R}} \mathrm{d}\phi \left\langle \phi' p'_\phi|\phi\right\rangle \langle \phi|\psi_{\phi,i}\rangle \,. \tag{3.95}$$

Expressing the $\sin\theta$ in exponential form the first integral is analytically solved to get

$$\int_{\mathbb{R}} \mathrm{d}\theta \sin\theta \,\langle \theta' p'_\theta|\theta\rangle \,\langle \theta|\psi_{\theta,i}\rangle = \frac{C_\theta}{2\mathrm{i}} \exp\left[\frac{-1}{2(\gamma_\theta+\gamma)}\right] \mathrm{e}^{g_\theta}\left(\mathrm{e}^{w} - \mathrm{e}^{-w}\right), \tag{3.96}$$

with the constant

$$C_\theta = \frac{\sqrt{2}\,(\gamma_\theta\gamma)^{1/4}}{\sqrt{\gamma_\theta+\gamma}},$$

the exponents

$$\begin{aligned} g_\theta(\theta', p'_\theta) &= -\frac{\gamma_\theta\gamma(\Delta\theta')^2}{2(\gamma_\theta+\gamma)} - \frac{1}{2(\gamma_\theta+\gamma)\hbar^2}\left[(\Delta p'_\theta)^2 - 2\mathrm{i}\hbar(\gamma_\theta p'_\theta + \gamma p_{\theta,i})\Delta\theta'\right], \\ w(\theta', p'_\theta) &= \frac{1}{\gamma_\theta+\gamma}\left[\frac{\Delta p'_\theta}{\hbar} + \mathrm{i}\left(\gamma\theta' + \gamma_\theta\theta_i\right)\right], \end{aligned}$$

and the definitions $\Delta\theta' = \theta' - \theta_i$ and $\Delta p'_\theta = p'_\theta - p_{\theta,i}$.

The overlap integral in the ϕ case gives the standard result

$$\int_{\mathbb{R}} \mathrm{d}\phi \left\langle \phi' p'_\phi|\phi\right\rangle \langle \phi|\psi_{\phi,i}\rangle = C_\phi \mathrm{e}^{g_\phi}, \tag{3.98}$$

with C_ϕ and g_ϕ obtained from exchanging θ by ϕ in the formulas for C_θ and g_θ.

With $\boldsymbol{z'} = \boldsymbol{z}_0$ the overlap $\langle \boldsymbol{z}_0|\Psi_i\rangle$ of the HK formula (3.91) is obtained. Since equation (3.96) contains two different terms, the autocorrelation function splits in two IVR integrals each with a different unnormalized initial distribution $D_{0_\pm}(z_0)$

$$\begin{aligned} \left|\langle \boldsymbol{z}_0|\Psi_i\rangle_\pm\right| &= \frac{C_\theta C_\phi}{2} D_{0_\pm}(z_0) \\ &= \frac{C_\theta C_\phi}{2} \exp\left\{\frac{-1}{2(\gamma_\theta+\gamma)} + \Re\left[g_\theta(\theta_0, p_{\theta,0}) + g_\phi(\phi_0, p_{\phi,0}) \pm w(\theta_0, p_{\theta,0})\right]\right\}. \end{aligned} \tag{3.99}$$

The overlaps $\langle \boldsymbol{z}_0|\Psi_i\rangle_\pm$ are written in terms of the initial distributions as

$$\langle \boldsymbol{z}_0|\Psi_i\rangle_\pm = \frac{C_\theta C_\phi}{2\mathrm{i}} D_{0_\pm}(z_0)\mathrm{e}^{\mathrm{i}\Phi_\pm(z_0)}, \tag{3.100}$$

with

$$\Phi_\pm(z_0) = \Im\left[g_\theta(\theta_0, p_{\theta,0}) + g_\phi(\phi_0, p_{\phi,0}) \pm w(\theta_0, p_{\theta,0})\right]. \tag{3.101}$$

The exponent in equation (3.99) can be simplified considering

$$\frac{-1}{2(\gamma_\theta+\gamma)} + \Re\left[g_\theta(\theta_0, p_{\theta,0}) \pm w(\theta_0, p_{\theta,0})\right] = -\frac{\gamma_\theta\gamma(\Delta\theta_0)^2}{2(\gamma_\theta+\gamma)} - \frac{(\Delta p_{\theta,0} \mp \hbar)^2}{2(\gamma_\theta+\gamma)\hbar^2}, \tag{3.102}$$

with $\Delta\theta_0 = \theta_0 - \theta_i$ and $\Delta p_{\theta,0} = p_{\theta,0} - p_{\theta,i}$. This, together with equation (3.98), and the definitions given above show that the initial distribution is made of two Gaussians centered at $z_i = (\theta_i, \phi_i, p_{\theta,i} \pm \hbar, p_{\phi,i})$ respectively.

The overlap at time t, $\langle \Psi_i|\boldsymbol{z}_t\rangle$, has the form

$$\langle \Psi_i|\boldsymbol{z}_t\rangle = \frac{C_\theta C_\phi}{-2\mathrm{i}} \exp\left[\frac{-1}{2(\gamma_\theta+\gamma)}\right] \mathrm{e}^{g^*_{\theta,t}}\mathrm{e}^{g^*_{\phi,t}}\left(\mathrm{e}^{w^*_t} - \mathrm{e}^{-w^*_t}\right), \tag{3.103}$$

with the same constants C_θ and C_ϕ defined above. The functions $g^*_{\theta,t}$, $g^*_{\phi,t}$, and w^*_t are the complex conjugate of the ones defined above and evaluated at $(\theta_t, p_{\theta,t})$.

The overall constant in the HK equation (3.91) is

$$N = \frac{1}{4\pi^2\hbar^2}\frac{C_\theta^2 C_\phi^2}{4}, \tag{3.104}$$

which is the the normalization constant for the initial distributions $D_{0_\pm}(z0)$, equation (3.99). This gives the normalized distributions $\bar{D}_{0\pm}(z_0)$

$$\bar{D}_{0_\pm}(z_0) = N D_{0_\pm}(z_0) \tag{3.105}$$

The autocorrelation function (3.91) it is written as

$$A_\Psi(t) = \frac{-2\mathrm{i}}{C_\theta C_\phi}\int \mathrm{d}z_0 \left[\bar{D}_{0_+}\mathrm{e}^{\mathrm{i}\Phi_+(z_0)} - \bar{D}_{0_-}\mathrm{e}^{\mathrm{i}\Phi_-(z_0)}\right] C_t(z_0)\mathrm{e}^{\mathrm{i}S_t(z_0)}\langle \Psi_i|\boldsymbol{z}_t\rangle, \tag{3.106}$$

where the $\bar{D}_{0_\pm} = \bar{D}_{0_\pm}(z_0)$. This integral is to be evaluated by Monte-Carlo using

$$A_\Psi(t) \approx \frac{-2\mathrm{i}}{C_\theta C_\phi}\left[\left\langle \mathrm{e}^{\mathrm{i}S_t(z_0)}\,\langle\Psi_i|\boldsymbol{z}_t\rangle\,\mathrm{e}^{\mathrm{i}\Phi_-(z_0)}\right\rangle_{\bar{D}_{0_+}} - \left\langle \mathrm{e}^{\mathrm{i}S_t(z_0)}\,\langle\Psi_i|\boldsymbol{z}_t\rangle\,\mathrm{e}^{\mathrm{i}\Phi_+(z_0)}\right\rangle_{\bar{D}_{0_-}}\right], \tag{3.107}$$

where the $\langle\ \rangle_{\bar{D}_{0_\pm}}$ means taking average of the quantity inside with distribution function $\bar{D}_{0_\pm}$. For each of the initial conditions sampled it is calculated the classical trajectory, the stability matrix, and the action; with these it is possible to get all the components of the HK formula (3.107). In practice this numerical integration is done in cartesian coordinates with the constraint of a particle lying all the time on the 2-sphere. This integration gives $\boldsymbol{x}_t = \boldsymbol{x}(\boldsymbol{x}_0, t)$, the trajectory in cartesian coordinates as a function of the initial conditions, which is easily transformed to spherical polar coordinates to get $\boldsymbol{z}_t = \boldsymbol{z}(\boldsymbol{z}_0, t)$, see formulas in appendix B.

For applications, using equation (3.107) is very inefficient, since a double sampling on phase space is necessary. If the initial Gaussian is narrow in configuration space, and if it is centered far from the poles, $\theta \approx \pi/2$, the most efficient way of obtaining the semiclassical autocorrelation function is to resort to Sun and Miller's initial state [48]. In fact, all the calculations shown in the next section were obtained using this method.

The stability matrix in spherical polar coordinates, $\partial\boldsymbol{z}_t/\partial\boldsymbol{z}_0$, is obtained from its analog in cartesian coordinates, $\partial\boldsymbol{x}_t/\partial\boldsymbol{x}_0$, using the chain rule

$$\frac{\partial\boldsymbol{z}_t}{\partial\boldsymbol{z}_0} = \frac{\partial\boldsymbol{z}_t}{\partial\boldsymbol{x}_t}\cdot\frac{\partial\boldsymbol{x}_t}{\partial\boldsymbol{x}_0}\cdot\frac{\partial\boldsymbol{x}_0}{\partial\boldsymbol{z}_0}. \tag{3.108}$$

The first factor is the Jacobian matrix of the transformation $\boldsymbol{z}(\boldsymbol{x})$ evaluated at time t on the trajectory, while the last factor is the Jacobian for the inverse transformation, $\boldsymbol{x}(\boldsymbol{z})$, evaluated at the initial conditions. Explicit formulas for these matrices can be found in the appendix C.

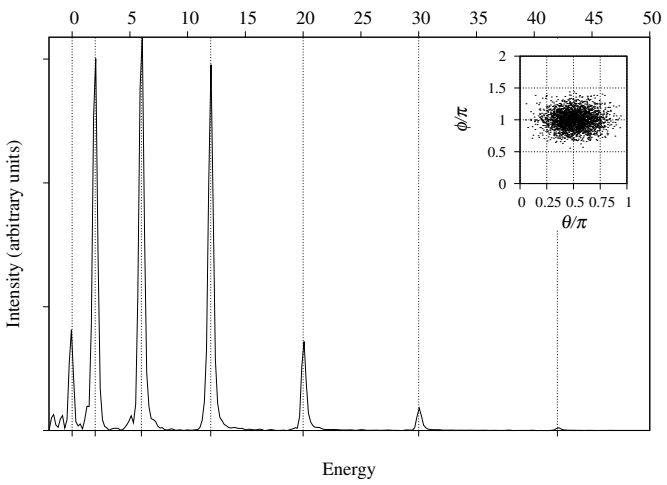

Figure 3.11: HK energy spectrum for a free 3D rotor. The vertical grid lines are set at the quantum energy levels: $E_J = J(J+1), J = 0, 1, 2, 3, ...$ The inset shows the distribution of initial conditions in configuration space.

3.6.1 Numerical Results

To be sure the method works, the semiclassical energy spectrum for a free 3D rotor was calculated. The results are shown in figure 3.11. There is a good agreement between the semiclassical peaks and the quantum energy levels

$$E_J = J(J+1), \qquad J = 0, 1, 2, 3, ..., \tag{3.109}$$

for $B = 1$ and $\hbar = 1$. The coherent states and initial wave function have the same width parameter, $\gamma = 10$. This value of γ makes possible to get the lowest energy levels; for larger values of γ higher energy peaks are obtained. The initial wave packet was centered at $(\theta_0, \phi_0, p_{\theta,0}, p_{\phi,0}) = (\pi/2, \pi, 0, 0)$. A total of 2500 classical trajectories were calculated with time step 10^{-3} and propagated for $2^{13} = 16,384$ steps, the initial conditions in configuration space can be seen in the inset of the figure. The autocorrelation function obtained was convoluted with a Gaussian

peak [51]

$$g_c(t) = G \exp\left\{\frac{-t^2}{2\sigma_c^2}\right\}, \tag{3.110}$$

centered at $t = 0$, with $G = 1$, and width $\sigma_c = 6$.

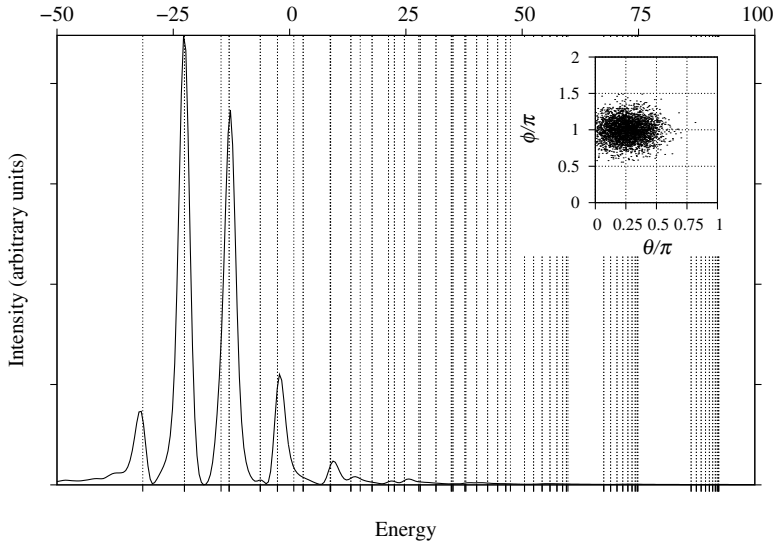

Figure 3.12: HK energy spectrum for a 3D rotor in a static electric field, $\omega = 40$, using $\gamma = 10$. The vertical grid lines are set at the quantum energy levels. The inset shows the initial distribution in configuration space.

For the 3D rotor in a static field, figure 3.12 shows the semiclassical spectrum for $\omega = 40$. All the width parameters are set to $\gamma = 10$, and the initial wave packet is centered at $(\theta_0, \phi_0, p_{\theta,0}, p_{\phi,0}) = (\pi/4, \pi, 0, 0)$. This is Gaussian wavepacket is relatively dispersed in configuration space, see inset of the figure, allowing to get the low energy region of the spectrum. A total of 10^5 trajectories were necessary with a time step of $\times 10^{-4}$ and propagated for $2^{13} = 65,536$ steps. To clean up the spectrum, the autocorrelation function was convoluted with a Gaussian peak (3.110) with $G = 1$ and $\sigma_c = 1$. Except by the second and fourth excited states there are peaks at the lowest energy quantum eigenstates.

To obtain the high energy spectrum it is necessary to use an initial Gaussian

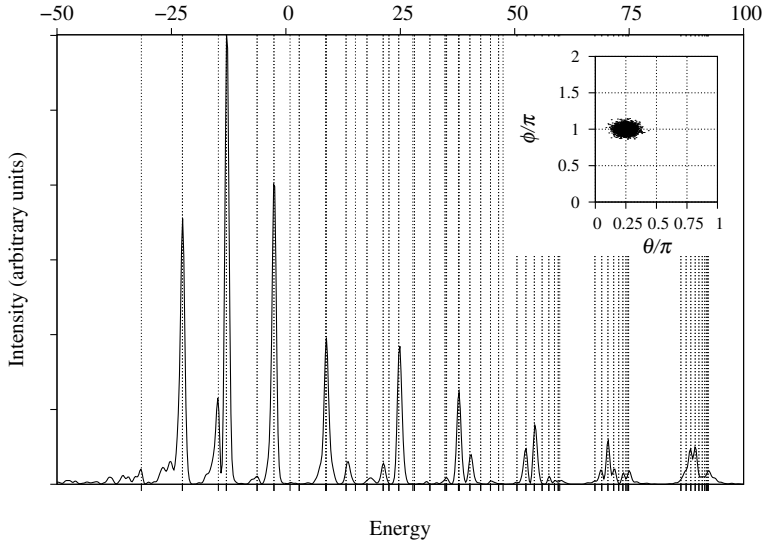

Figure 3.13: HK energy spectrum for a 3D rotor in a static electric field, $\omega = 40$, using $\gamma = 100$. The vertical grid lines are set at the quantum energy levels. The inset shows the initial distribution in configuration space.

wave packet narrower in configuration space but wider in momentum space. For width $\gamma = 100$ the spectrum for $\omega = 40$ is shown in figure 3.13, the inset shows an initial distribution narrower in configuration space than the one for $\gamma = 10$. For this spectrum a total of 10^5 trajectories were propagated during 2^{14} time steps. Since the trajectories are faster on average, the time step was reduced to 10^{-4}. For the convolution, it was used $G = 1$ and $g_c = 2.50$ to obtain a cleaner spectrum. In the figure it is possible to see that there is a peak at the third eigenvalue, and some of the higher energy peaks are at the correct position. It is interesting to see that the clustering of quantum states is correctly obtained for energies larger than 50.

In a laser field for $\Delta\omega = 10$, the spectrum can be seen in figure 3.14. The width parameters are $\gamma = 100$ and the initial wave function is centered at $(\theta_0, \phi_0, p_{\theta,0}, p_{\phi,0}) = (\pi/2, \pi, 10, 0)$. For this high value of $p_{\theta,0}$ most of the trajectories will have enough

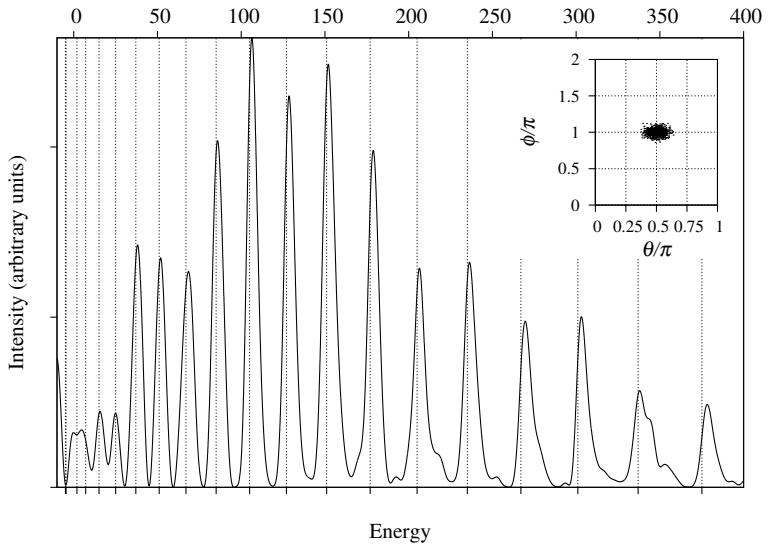

Figure 3.14: HK energy spectrum for a 3D rotor in laser field, $\Delta\omega = 10$. The vertical grid lines are set at the quantum energy levels. Excellent agreement is found except at the lowest energy levels. These results are for $\gamma = 100$, and the initial wave packed centered at $(\theta_0, \phi_0, p_{\theta,0}, p_{\phi,0}) = (\pi/2, \pi, 10, 0)$. The inset shows the initial conditions distribution in configuration space.

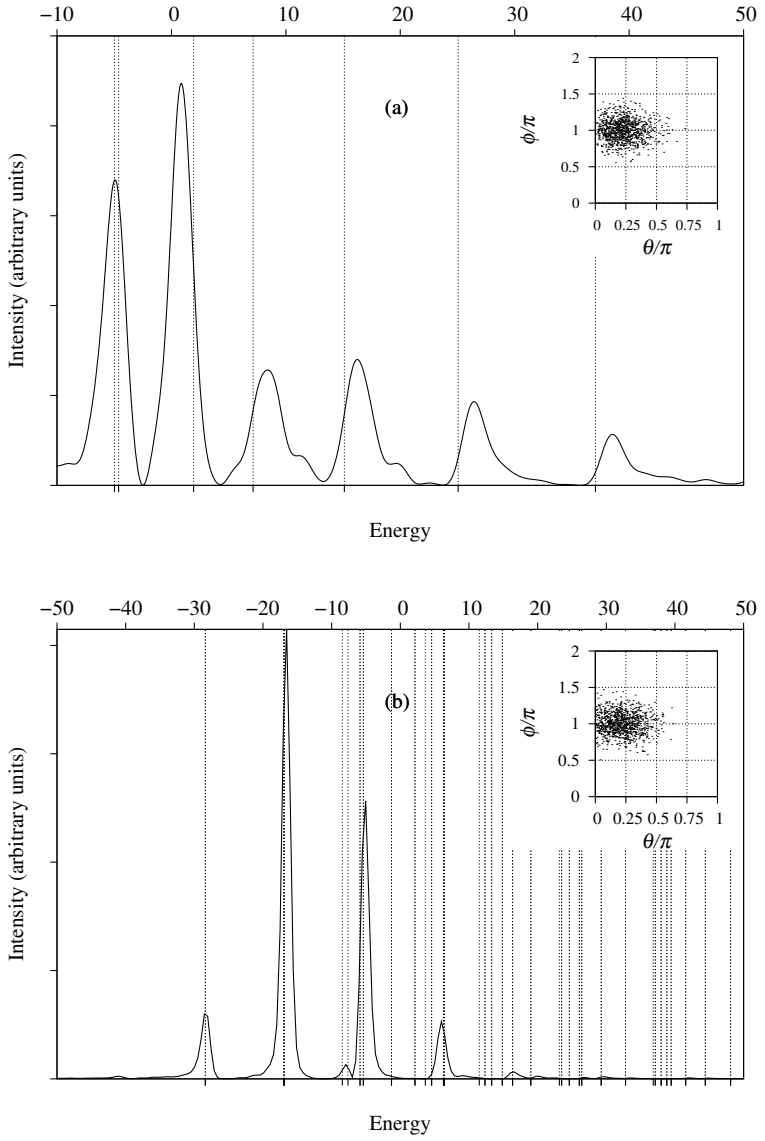

Figure 3.15: HK energy spectrum for a 3D rotor in laser field: (a) $\Delta\omega = 10$, (b) $\Delta\omega = 40$. The vertical grid lines are set at the quantum energy levels. The initial wave packed was centered at $(\theta_0, \phi_0, p_{\theta,0}, p_{\phi,0}) = (\pi/5, \pi, 0, 0)$ in both cases. In the insets can be seen the distribution of initial conditions in configuration space.

energy to go over the effective potential barrier. This spectrum agrees well with the quantum levels except for low energy. A total of 1000 trajectories were used with a time step of 5×10^{-4} and propagated for $2^{13} = 65,536$ steps. The convolution of the autocorrelation function was performed with a wider Gaussian peak, $G = 1$ and $\sigma_c = 0.4$, which produces an spectrum with wider peaks than figures 3.12-3.13.

In figure 3.15 we can observe the low energy part of the spectrum. This was calculated for $\gamma = 10$ and initial wave packet at $(\theta_0, \phi_0, p_{\theta,0}, p_{\phi,0}) = (\pi/5, \pi, 0, 0)$. In the panel (a), for $\Delta\omega = 10$, the spectrum presents peaks qualitatively fine at the quantum eigenvalues, it was used a Gaussian with $g_c = 1.25$ in the convolution. For the second panel, $\Delta\omega = 40$, the agreement with the quantum eigenvalues is better although less peaks are shown in the spectrum, in this case $g_c = 2$ was used to convolute the autocorrelation function.

For collinear fields with $\omega = 10$ and $\Delta\omega = 40$ the semiclassical spectrum is shown in the figure 3.15. This spectrum was obtained using $\gamma = 1$ and initial wavefunction at $(\theta_0, \phi_0, p_{\theta,0}, p_{\phi,0}) = (\pi/2, \pi, 0, 0)$. For this γ the initial wave packet is very wide in configuration space as can be seen in the inset of the figure. The lower energy part of the spectrum agrees very nicely with the first 4 quantum levels. Although the fifth energy level does not appear in the spectrum, levels 6 and 7 show a good agreement. This time 1000 trajectories were employed with a time step of 10^{-4} and propagated for $2^{14} = 131072$ steps. This smaller time step was needed to accomplish better numerical accuracy in the propagation of the stability matrix. The autocorrelation function was convoluted using a Gaussian peak with $G = 1$ and $\sigma_c = 2.5$.

The high energy region of the spectrum is shown in figure 3.16. This spec-

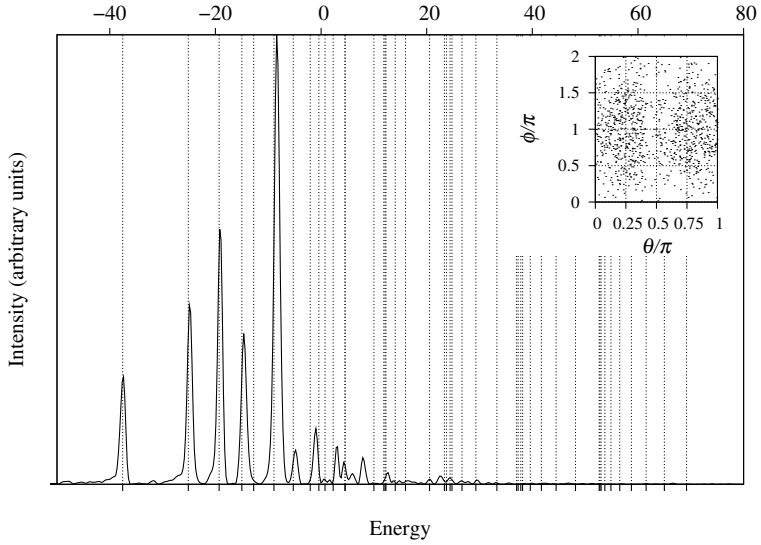

Figure 3.16: HK energy spectrum for a 3D rotor in collinear fields, $\omega/\Delta\omega = 10/40$. The vertical grid lines are set at the quantum energy levels. Initial wave packet with $\gamma = 100$, and centered at $(\theta_0, \phi_0, p_{\theta,0}, p_{\phi,0}) = (\pi/2, \pi, 10, 0)$. Distribution of initial conditions in configuration space shown in the inset.

trum was obtained for a width $\gamma = 10$ and an initial wavefunction centered at $(\theta_0, \phi_0, p_{\theta,0}, p_{\phi,0}) = (\pi/2, \pi, 5, 0)$. For this spectrum were used 10,000 trajectories with a time step of 5×10^{-4} and run for $2^{13} = 65,536$ time steps. The convolution this time is made with parameters $\sigma_c = 1$ and $G = 1$. The spectrum has very wide peaks centered at the energies where the quantum eigenstates tend to cluster together.

Finally, in tilted fields the results are shown in figures 3.18 and 3.19 for $\omega/\Delta\omega = 1/4$ and $\beta = \pi/4$. The first figure present the spectrum for a very wide initial wave function, $\gamma = 1$, and centered at $(\theta_0, \phi_0, p_{\theta,0}, p_{\phi,0}) = (\pi/2, \pi, 0, 0)$. For convolution it was used a Gaussian of width $\sigma_c = 1.5$. The autocorrelation function was obtained averaging over 10^5 trajectories, and with a small time step to guarantee the precision of the numerical integration. Even for this relatively large number

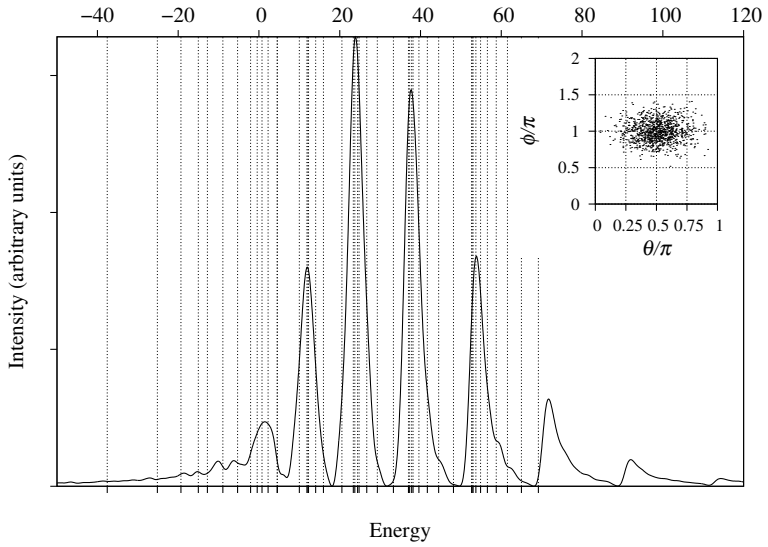

Figure 3.17: HK energy spectrum for a 3D rotor in collinear fields, $\omega/\Delta\omega = 10/40$. The vertical grid lines are set at the quantum energy levels. Initial wave packet with $\gamma = 10$, and centered at $(\theta_0, \phi_0, p_{\theta,0}, p_{\phi,0}) = (\pi/5, \pi, 0, 0)$. Distribution of initial conditions in configuration space shown in the inset.

of trajectories the autocorrelation function was not sufficiently smooth as a time function. The spectrum shows good agreement for the ground level, for the low energy excited states are obtained wide peaks covering more than one quantum state. For high energy the results are inconclusive.

In the high energy spectrum, figure 3.19, the initial wave function has $\gamma = 10$ and it is centered at $(\theta_0, \phi_0, p_{\theta,0}, p_{\phi,0}) = (\pi/2, \pi, 5, 0)$. The spectrum was obtained convoluting the autocorrelation function with a $\sigma_c = 1$ Gaussian. A total of 10^5 trajectories were propagated. The final autocorrelation function was not a smooth function of time, indicating that a larger number of trajectories is needed. The final spectrum shows a qualitative agreement with the eigenenergies with wide peaks over the energies where the quantum levels cluster together. The low energy region is useless.

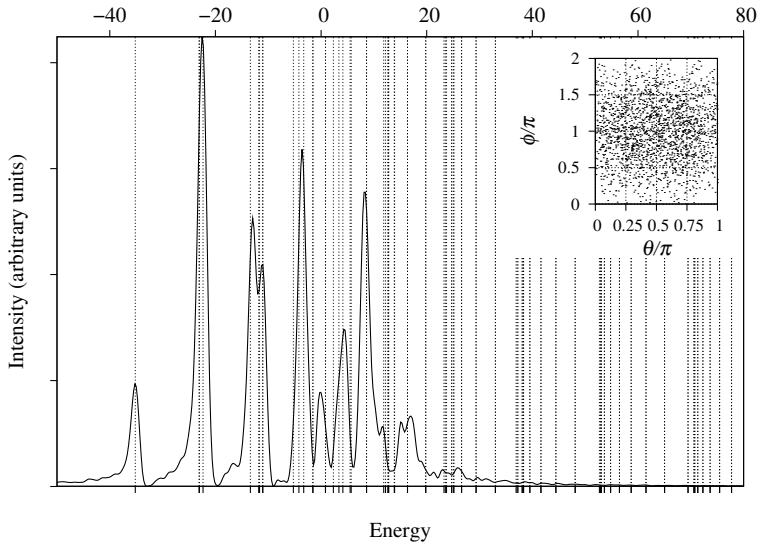

Figure 3.18: HK energy spectrum for a 3D rotor in tilted fields, $\omega/\Delta\omega = 10/40$, $\beta = \pi/4$. The vertical grid lines are set at the quantum energy levels. Initial wave packet with $\gamma = 10$, centered at $(\theta_0, \phi_0, p_{\theta,0}, p_{\phi,0}) = (\pi/5, \pi, 0, 0)$. Inset shows the the initial conditions distribution in configuration space.

In conclusion, the Herman-Kluk method works fine when the target spectrum has well separated quantum levels, or if the objective is to get a rough idea of the energy density. The method works better for larger values of ω and/or $\Delta\omega$ and small β. The nonintegrability brings some problems to the calculation of the autocorrelation function. For a highly nonintegrable case, like $\beta = \pi/4$, and using 10^5 initial conditions, the autocorrelation function is not sufficiently smooth as a function of time. This is indicating that more trajectories are needed in the initial sampling. For this number of trajectories, 10^5, the calculation takes 15 hours in average, increasing the number of trajectories will increase the calculation time linearly. It could be reasonable to run 10^6 initial conditions which would take almost a week of CPU[1] time.

[1]AMD Athlon XP 3000+ processor at 2.16 GHz.

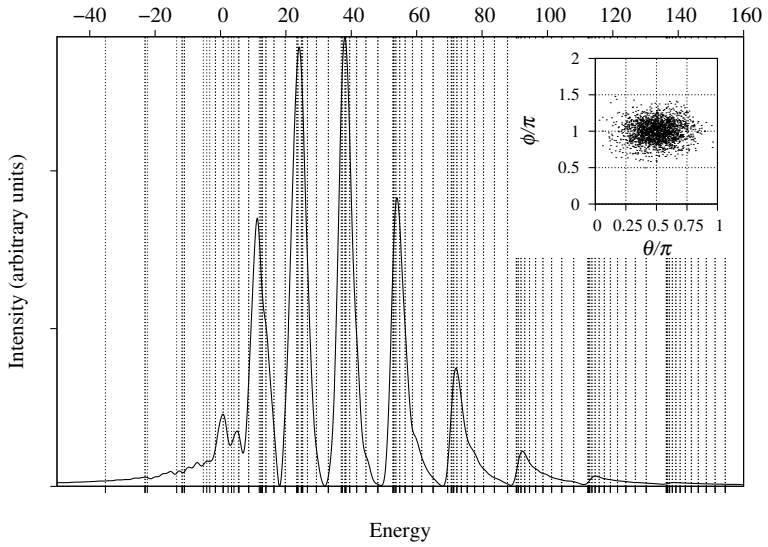

Figure 3.19: HK energy spectrum for a 3D rotor in tilted fields, $\omega/\Delta\omega = 10/40$, $\beta = \pi/4$. The vertical grid lines are set at the quantum energy levels. Initial wave packet with $\gamma = 10$, centered at $(\theta_0, \phi_0, p_{\theta,0}, p_{\phi,0}) = (\pi/5, \pi, 5, 0)$. Inset shows the the initial conditions distribution in configuration space.

3.7 A HK-Type Propagator in Terms of Rotational Coherent States

The use of harmonic oscillator coherent states (HOCS) limits the applicability of the HK method to systems with cartesian degrees of freedom (Euclidean configuration space) [49, 86]. We have seen that the HK method can be extended to rotational problems defining periodic coherent states [49, 80, 87] and using a very large value of γ with a properly defined initial wave function [48, 49, 86]. A nicer approach for rotational problems would be to obtain a HK-type propagator in terms of rotational coherent states (RCS) instead of HOCS. In our approach we first define RCS in a similar fashion to those in references [52, 53] and them following Miller's procedure in reference [55] we will try to get the HK prefactor for

RCS.

3.7.1 Rotational Coherent States

The eigenfunctions of a diatomic rotor are the spherical harmonics $Y_M^J(\theta,\phi) = \langle\theta,\phi|JM\rangle$, characterized by quantum numbers J and M for the total angular momentum and its projection into the lab-fixed z-axis respectively. We are particularly interested in the eigenstates with $M = J$, $\langle\theta,\phi|JJ\rangle$, since these are minimum uncertainty wave functions [52]. In classical terms, for these states the angular momentum vector is aligned with the lab-fixed z-axis, $\theta = \pi/2$, and ϕ can have any possible value in $[0, 2\pi)$.

Let $(\bar{x},\bar{y},\bar{z})$ be a cartesian frame where the angular momentum vector is aligned with the $\bar{z}$-axis, and the (free) rotor moves on the $\bar{x}\bar{y}$-plane with the $\bar{x}$-axis forming the smallest angle with the z-axis along the intersection of the $z\bar{z}$ and $\bar{x}\bar{y}$ planes. The barred frame is obtained applying three successive Euler rotations on the lab-frame, in terms of the rotor's action-angle variables and the rotation operators (see appendix F) this transformation is performed by

$$\begin{aligned}\hat{R}(q_m,\bar{\theta},q_j) &= \hat{R}(q_j,z'')\hat{R}(\bar{\theta},y')\hat{R}(q_m,z)\\ &= \hat{R}(q_m,z)\hat{R}(\bar{\theta},y)\hat{R}(q_j,z)\\ &= \mathrm{e}^{-\mathrm{i}q_m\hat{J}_z}\mathrm{e}^{-\mathrm{i}\bar{\theta}\hat{J}_y}\mathrm{e}^{-\mathrm{i}q_j\hat{J}_z},\end{aligned} \tag{3.111}$$

q_j and q_m are the usual angle variables, j and m the respective action variables, and $\bar{\theta} = \arccos(m/j)$ is the angle between the lab-fixed z-axis and the angular momentum vector.

Let $|J,\boldsymbol{\alpha}\rangle \equiv \left|J,q_m,\bar{\theta},q_j\right\rangle$ be the state defined by applying the rotation operator

$\hat{R}(\boldsymbol{\alpha}) \equiv \hat{R}(q_m, \bar{\theta}, q_j)$ on the $|JJ\rangle$ state. Using the results in appendix F we have

$$\begin{aligned} |J, \alpha\rangle &\equiv \hat{R}(\boldsymbol{\alpha})\,|JJ\rangle \\ &= \sum_{M=-J}^{J} |JM\rangle\, D^J_{MJ}(\boldsymbol{\alpha}) \\ &= \sum_{M=-J}^{J} |JM\rangle\, d^J_{MJ}(\bar{\theta}) \mathrm{e}^{-\mathrm{i}(Jq_j + Mq_m)}, \end{aligned} \tag{3.112}$$

with the Wigner's d-function, $d^J_{MJ}(\bar{\theta})$, defined in appendix F. The $\left|J, q_m, \bar{\theta}, q_j\right\rangle$ states are highly localized in q_m and $\bar{\theta}$, and completely delocalized in the q_j angle. If a $|JJ\rangle$ state is rotated by $\hat{R}(\boldsymbol{\alpha}(0))$, the obtained state: $|J, \boldsymbol{\alpha}(0)\rangle$ can be thought as a wave packet at $\boldsymbol{\alpha}(0) = (q_j(0), q_m(0), j(0), m(0))$ in the action-angle space. For this initial condition the classical trajectory is given by $\boldsymbol{\alpha}(t, \boldsymbol{\alpha}(0)) = (q_j(t), q_m(t), j(t), m(t))$, with each of the action-angle variables at time t depending also on the initial condition. Applying the time dependent rotation $\hat{R}(\boldsymbol{\alpha}(t))$ to the $|J, \boldsymbol{\alpha}(0)\rangle$ state, it is obtained a wave packet that rotates according to classical mechanics [52].

The overlap between two $|J, \boldsymbol{\alpha}\rangle$ states is given by the expression

$$\langle J, \boldsymbol{\alpha}'|J, \boldsymbol{\alpha}\rangle = \sum_{M=-J}^{J} D^J_{MJ}(\boldsymbol{\alpha}')^* D^J_{MJ}(\boldsymbol{\alpha}), \tag{3.113}$$

which is zero for states with different J, and one for identical states.

In analogy with reference [53] we shall use the RCS defined by

$$\begin{aligned} |z_t\rangle &= \mathrm{e}^{\mathrm{i}\mu - j/2} \sum_{J\geq 0} \frac{j^{J/2}}{\sqrt{J!}} \hat{R}(\boldsymbol{\alpha})\,|JJ\rangle \\ &= \mathrm{e}^{\mathrm{i}\mu - j/2} \sum_{J\geq 0} \sum_{M=-J}^{J} |JM\rangle\, \frac{j^{J/2}}{\sqrt{J!}} D^J_{MJ}(\boldsymbol{\alpha}), \end{aligned} \tag{3.114}$$

with $\boldsymbol{\alpha} = \left(q_m, \bar{\theta}, q_j\right)$ following the classical trajectory, and μ as an arbitrary real time dependent phase. In analogy to the HOCS, these RCS follow a Poisson

distribution in J

$$|\langle JM|z_t\rangle|^2 = \frac{j^J}{J!}\mathrm{e}^{-j}. \tag{3.115}$$

The overlap of two RCS (3.114) is

$$\begin{aligned}\langle z_t'|z_t\rangle &= \mathrm{e}^{\mathrm{i}\Delta\mu-\bar{\jmath}}\sum_{JJ'}\frac{j^{J/2}}{\sqrt{J!}}\frac{j'^{J'/2}}{\sqrt{J'!}}\langle J'J'|\,\hat{R}(\boldsymbol{\alpha}')^{-1}\hat{R}(\boldsymbol{\alpha})\,|JJ\rangle \\ &= \mathrm{e}^{\mathrm{i}\Delta\mu-\bar{\jmath}}\sum_{JJ'}\frac{j^{J/2}}{\sqrt{J!}}\frac{j'^{J'/2}}{\sqrt{J'!}}\langle J'J'|\,\hat{R}(\tilde{\boldsymbol{\alpha}})\,|JJ\rangle \\ &= \mathrm{e}^{\mathrm{i}\Delta\mu-\bar{\jmath}}\sum_{J}\frac{\tilde{\jmath}}{J!}D^J_{JJ}(\tilde{\boldsymbol{\alpha}}).\end{aligned} \tag{3.116}$$

with $\bar{\jmath} = (j+j')/2$, $\tilde{\jmath} = \sqrt{jj'}$, and $\Delta\mu = \mu - \mu'$. In the second line it is used the combined rotation $\hat{R}(\tilde{\boldsymbol{\alpha}}) \equiv \hat{R}(\boldsymbol{\alpha}')^{-1}\hat{R}(\boldsymbol{\alpha})$. Using equation (F.13) in appendix F, the overlap is rewritten as

$$\begin{aligned}\langle z_t'|z_t\rangle &= \mathrm{e}^{\mathrm{i}\Delta\mu-\bar{\jmath}}\sum_{J}\frac{\tilde{\jmath}^J}{J!}D^1_{1,1}(\tilde{\boldsymbol{\alpha}})^J \\ &= \exp\left[\mathrm{i}\Delta\mu - \bar{\jmath} + \tilde{\jmath}D^1_{1,1}(\tilde{\boldsymbol{\alpha}})\right]\end{aligned} \tag{3.117}$$

This RCS (3.114) can be inserted into Schrödinger's equation to give

$$\mathrm{i}\hbar\frac{\partial}{\partial \mathrm{t}}\,|z_t\rangle = \hat{H}\,|z_t\rangle\,. \tag{3.118}$$

In general, the Hamiltonian for a diatomic rotor in external fields can be written as

$$\hat{H} = B\hat{J}^2 + V(\hat{q}_m, \hat{\theta}, \hat{q}_j), \tag{3.119}$$

with B as the rotational constant, $\hat{J}^2$ as the operator for the square of the angular momentum, and $\hat{q}_m$, $\hat{\theta}$, and $\hat{q}_j$ as operators. Multiplying on the left by $\langle z_t'|$ is obtained

$$\mathrm{i}\hbar\,\langle z_t'|\,\frac{\partial}{\partial \mathrm{t}}\,|z_t\rangle = \langle z_t'|\,\hat{H}\,|z_t\rangle\,. \tag{3.120}$$

Using the RCS of equation (3.114) the derivative on the LHS of (3.118) becomes (see appendix G)

$$\frac{\partial}{\partial \mathrm{t}}\left|z_t\right\rangle = \left(\mathrm{i}\dot{\mu} - \frac{1}{2}\frac{\mathrm{d}j}{\mathrm{d}t}\right)\left|z_t\right\rangle + \mathrm{e}^{\mathrm{i}\mu - j/2}\sum_{JM}\left|JM\right\rangle \frac{j^{J/2}}{\sqrt{J!}} D^J_{MJ}(\boldsymbol{\alpha})\left(J\bar{F} + MG\right), \quad (3.121)$$

with the functions $\bar{F}$ and G

$$\bar{F} = \frac{1}{2j}\frac{\mathrm{d}j}{\mathrm{d}t} + \frac{m/j}{j^2 - m^2}\left(m\frac{\mathrm{d}j}{\mathrm{d}t} - j\frac{\mathrm{d}m}{\mathrm{d}t}\right) - \mathrm{i}\dot{q}_j, \quad (3.122a)$$

$$G = -\frac{1}{j^2 - m^2}\left(m\frac{\mathrm{d}j}{\mathrm{d}t} - j\frac{\mathrm{d}m}{\mathrm{d}t}\right) - \mathrm{i}\dot{q}_m. \quad (3.122b)$$

Multiplying on the left by $\langle z'_t|$ is obtained the matrix element on the LHS of equation (3.120)

$$\langle z'_t|\frac{\partial}{\partial \mathrm{t}}\left|z_t\right\rangle = \left(\mathrm{i}\dot{\mu} - \frac{1}{2}\frac{\mathrm{d}j}{\mathrm{d}t}\right)\langle z'_t|z_t\rangle + \mathrm{e}^{\mathrm{i}\Delta\mu - \bar{\jmath}}\sum_{JM}\frac{\tilde{\jmath}^J}{J!} D^J_{MJ}(\boldsymbol{\alpha}')^* D^J_{MJ}(\boldsymbol{\alpha})\left[J\bar{F} + MG\right] \quad (3.123)$$

As shown in appendix G, equation (3.123) can be simplified to get

$$\langle z'_t|\frac{\partial}{\partial \mathrm{t}}\left|z_t\right\rangle = \langle z'_t|z_t\rangle\left[\mathrm{i}\dot{\mu} - \frac{1}{2}\frac{\mathrm{d}j}{\mathrm{d}t} + \tilde{\jmath}\left(\bar{F}D^1_{1,1}(\tilde{\boldsymbol{\alpha}}) + \mathrm{i}G\frac{\partial}{\partial q_m}D^1_{1,1}(\tilde{\boldsymbol{\alpha}})\right)\right] \quad (3.124)$$

The action of the $\hat{J}^2$ on the RCS $\left|z_t\right\rangle$ gives (appendix G)

$$\begin{aligned}\hat{J}^2\left|z_t\right\rangle &= \mathrm{e}^{\mathrm{i}\mu - j/2}\sum_{J\geq 0}\sum_{M=-J}^{J}\hat{J}^2\left|JM\right\rangle\frac{j^{J/2}}{\sqrt{J!}}D^J_{MJ}(\boldsymbol{\alpha}) \\ &= \mathrm{e}^{\mathrm{i}\mu - j/2}\sum_{J\geq 0}\sum_{M=-J}^{J}J(J+1)\left|JM\right\rangle\frac{j^{J/2}}{\sqrt{J!}}D^J_{MJ}(\boldsymbol{\alpha}).\end{aligned} \quad (3.125)$$

Now multiplying on the left by $\langle z'_t|$ is obtained

$$\begin{aligned}\langle z'_t|\hat{J}^2\left|z_t\right\rangle &= \mathrm{e}^{\mathrm{i}\Delta\mu - \bar{\jmath}}\sum_{J}J(J+1)\frac{\tilde{\jmath}}{J!}D^J_{JJ}(\tilde{\boldsymbol{\alpha}}) \\ &= \mathrm{e}^{\mathrm{i}\Delta\mu - \bar{\jmath}}\sum_{J}\frac{J(J+1)}{J!}\left[\tilde{\jmath}D^1_{1,1}(\tilde{\boldsymbol{\alpha}})\right]^J.\end{aligned} \quad (3.126)$$

After doing similar manipulations as in equation (3.124), the result above simplifies nicely to (appendix G)

$$\langle z'_t|\hat{J}^2\left|z_t\right\rangle = \tilde{\jmath}D^1_{1,1}(\tilde{\boldsymbol{\alpha}})\left[\tilde{\jmath}D^1_{1,1}(\tilde{\boldsymbol{\alpha}}) + 2\right]\langle z'_t|z_t\rangle. \quad (3.127)$$